Recent Advances in the Modeling of the Impact of Nonlinear Fiber Propagation Effects on Uncompensated Coherent Transmission Systems

Recent Advances in the Modeling of the Impact of Non-Linear Fiber Propagation Effects on Uncompensated Coherent Transmission Systems

P. Poggiolini and Y. Jiang

(Tutorial Review)

***Abstract*—The last few years have seen a wealth of new non-linear propagation modeling results appear in the literature, especially regarding coherent systems operating in the absence of optical dispersion compensation. One of the most prolific lines of research, though not the only one, has been that of improvements and upgrades to the GN-model, which have also led to the so-called EGN-model. In addition, many specific aspects of non-linear propagation, including format and symbol-rate dependence of non-linearity generation, long-correlated nonlinear phase and polarization noise, the effect of co-propagating amplified spontaneous emission noise and distributed amplification, and still others, have been focused on and several new related results have been published.**

This has been a very positive trend but, from the viewpoint of the end-users, such as system and network designers, this large body of new knowledge may have been found difficult to sort out. The question of when and whether more sophisticated models are truly needed in any given system/network scenario, for a given set of accuracy and computational complexity constraints, then naturally arises. This paper tries to address this practical issue and provide indications regarding possible effective solution to varied end-users' requirements.

***Index Terms*—coherent systems, uncompensated transmission, non-linear effects, GN-model, EGN-model**

I. Introduction

THE availability of *effective* models to assess the impact of non-linear fiber propagation on coherent optical communications systems is a key facilitating element in the planning, design and management of such systems and of the networks hosting them. For a model to be 'effective', it has to fulfill essentially two requirements: acceptable computational complexity and sufficient accuracy.

In recent years various models have been proposed in an effort to comply with these requirements. An extensive bibliography on modeling can be found in [1], [2]. Focusing on uncompensated transmission (UT) systems (i.e., systems not using *optical* chromatic dispersion compensation), among the many proposals the Gaussian-Noise model (or GN-model) has enjoyed widespread adoption and utilization in many different contexts, ranging from system analysis and design, to network optimization and control. On the other hand, recently, various limitations and shortcomings of the GN-model have been pointed out. In particular, certain peculiar 'specific aspects' of non-linearity generation are not resolved by the GN-model, or are not accurately accounted for. Among them, format-dependence of non-linearity generation, long-correlated nonlinear phase and polarization noise, non-linearity mitigation by Symbol Rate Optimization (SRO), the impact of co-propagating Amplified Spontaneous Emission (ASE) noise, the depletion of signal power, some aspects of distributed amplification, and yet others.

To address the GN-model limitations and better account for the effects listed above, sophisticated new models have been proposed. As a whole, a wealth of modeling results have been published especially over the last three years (see all references since 2013 to date, at the end of this paper) and this strong trend is continuing.

Such large body of new knowledge on modeling is very important and constitutes very substantial progress. At the same time, from the viewpoint of the end-users, like for instance system and network designers, the many new modeling solutions may appear difficult to sort out. Also, the adoption of more powerful models typically implies loss of ease of use and greater computational complexity. This leads to the question of when and whether more sophisticated models are truly needed in any given system/network scenario, for any given set of accuracy and computational complexity constraints. This paper tries to address these general emerging issues in a comprehensive way, from the viewpoint of the end-users' practical need for an effective solution to their specific modeling requirements.

Our general approach was to first identify very broad, encompassing sets of reference test system configurations. We considered five modulation formats (PM-QPSK, and PM-QAM with 8, 16, 32 and 64 constellation points), three fiber types (SMF, PSCF and NZDSF), three channel spacings, and both terrestrial-type and submarine-type span-lengths[1]. In these reference configurations we assessed the effectiveness of various modeling solutions, in terms of their complexity vs. accuracy trade-off. In the same scenarios, or suitable subsets thereof, the impact of the many previously listed 'specific aspects' of non-linear propagation, was also appraised, and possible modeling solutions discussed.

P. Poggiolini is with Politecnico di Torino, Dipartimento di Elettronica e Telecomunicazioni (DET), Corso Duca degli Abruzzi 24, 10129, Torino, Italy. Website: www.optcom.polito.it, e-mail: pierluigi.poggiolini@polito.it. Y. Jiang is with Dalian University, College of Information Engineering, Str. Xuefu Dajie 10, 116622, Dalian, China, e-mail jiangyanchao@dlu.edu.cn .

[1]All acronyms and definitions appearing in the paper are defined in a comprehensive list reported at the end, as Appendix A. The less common are also defined where they appear for the first time.

To the best of our knowledge, this paper represents one of the most extensive and encompassing such studies to date, with one important limitation: we focused chiefly on the GN and EGN-models, and recent evolutions and variants thereof. The reason of this choice was the GN-model widespread use, which definitely commanded an in-depth critical re-testing of it, carried out to a substantially wider and deeper extent than previously done. The EGN-model is a direct upgrade to the GN-model but, besides this circumstance, it truly represents very significant progress over the GN-model. So it seemed appropriate to concentrate on it, too. At the end of the paper, we briefly discuss other modeling approaches, which have emerged and may be advantageous or better suited, depending on specific modeling requirements.

In detail, Sect. II is devoted to the GN model. It contains a brief note on its origins, and a summary of its main equations and features for its various versions, including approximate closed-form ones. Following, an in-depth accuracy test is performed on the reference scenarios.

In Sect. III the *enhanced* GN model, or EGN model, is dealt with, following a similar pattern as for the GN-model in Sect. II. In addition, a specific subsection is devoted to the dependence of non-linearity generation on modulation format and symbol rate, a context in which, differently from the GN model, the EGN model provides highly accurate results.

In Sect. IV, the topic of long-correlated phase and polarization noise is confronted with. The actual impact of this specific aspect of NLI generation on the reference scenarios is assessed and its possible modeling solutions are discussed.

Sect. V examines two further NLI generation specific aspects which are often considered 'second-order' ones, namely the impact of co-propagating ASE noise and signal power depletion.

Sect. VI looks at modeling NLI in distributed-amplification systems, an important emerging topic given the increasing adoption of Raman amplifiers, either in hybrid solutions with EDFAs, or alone.

Sect. VII discusses other modeling approaches than GN or EGN-related ones, also in relation to the the issue of specifically singling-out phase and polarization noise, and of short links using very-high-cardinality formats.

Comments and conclusion follow.

II. The GN-model

A comprehensive tutorial presentation on the GN-model can be found in [1]. For the readers' convenience, here we summarize some background information.

Regarding bibliography, a diagram of the main GN-model-related papers till 2013 is shown in Fig. 1, with oldest at the top and most recent at the bottom. The denomination GN-model was first proposed in [9], but the first instance of a similar model can be traced back to the 1994 ECOC paper [3], shown at the top of the diagram. Note that the general ideas underpinning the GN-model appear to have emerged repeatedly and likely independently over the years, at least until 2011. Afterwards, publications are all related and extensively reference each other.

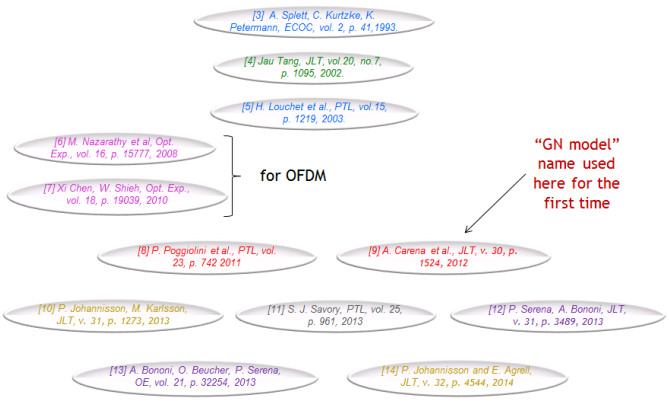

Fig. 1. Some of the main papers proposing GN-model-like approaches, till 2014, from oldest at the top to most recent at the bottom. For a more complete bibliography, see [1], [2].

The GN-model 'family' of Fig. 1 is just one of many non-linearity model families that have appeared throughout the history of optical communications (see [2] for an extended bibliography, and Sect. VII of this paper). Some of those many models are more sophisticated and intrinsically more accurate than the GN-model. What may tentatively justify the GN-model current widespread adoption is that perhaps it strikes a favorable balance between accuracy, complexity and ease of use. Whether such balance is indeed favorable, is one of the issues that this paper tries to address in the following.

In the general classification of models, the GN-model is a first-order regular-perturbation model, based on the Manakov non-PMD equation, that is Eq. (12) in [15] with the right-hand side set to zero. What is distinctive about the GN-model, and both represents an asset and a liability, is the assumption that each WDM channel can be treated as Gaussian noise (spectrally shaped as the signal). The justification of this approximation is pictorially provided by Fig. 2. A 32-GBaud 16QAM signal (left plot) is launched into SMF and, assuming UT (uncompensated transmission, that is the absence of optical chromatic dispersion compensation), already after 400 km the signal constellation has been transformed into the right plot, whose statistical distribution is found to be very close to Gaussian.

On the other hand, as it has been pointed out in [20], the dispersed signal is only first-order Gaussian, whereas multiple samples of the signal *do not* have a jointly-Gaussian distribution. The GN-model neglects this aspect and assumes that the signal is a jointly-Gaussian process. This approximation is an asset because it makes the model very simple. It is a liability because it causes some error, whose extent needs to be assessed.

As a final introductory remark, it is useful to provide some retrospective context. It was not until 2007-2008 that it became clear that the 'coherent revolution' would definitely take place. It then soon turned out that, surprisingly, the optimum dispersion management for coherent systems was *no optical dispersion compensation*, or UT. This was new and uncharted territory. It could have been explored using split-step simulations but, especially back then, with limited effec-

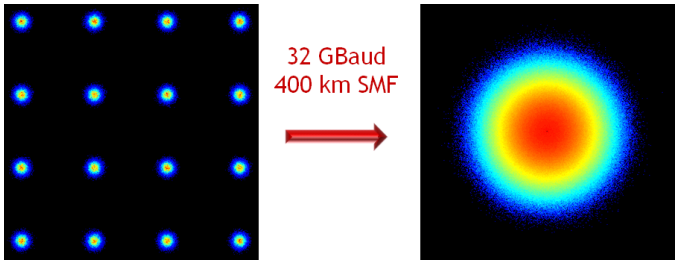

Fig. 2. Left: a 32-GBaud 16QAM signal at launch (a small amount of noise was added in the simulation to make the constellation points clearly visible). Right: the same signal after simulated propagation through 400 km of SMF, in linearity, without any dispersion compensation. Color coding is decreasing probability going from red to blue.

tiveness. To make sense of this new situation, a practical and manageable non-linearity estimation tool was urgently needed. Its accuracy should be good, but perfection was not required and could be traded off for effectiveness. It is this urgent need that explains why the GN-model rapidly caught on, when it was proposed for UT coherent optical systems in [8]-[9] supported by substantial simulative validation. Incidentally, the main reason why its earlier versions [3]-[5] had not been equally successful in the community is that the GN-model simply did not work well with the dispersion-managed IM/DD systems of the time, being UT an essential pre-requisite for the GN model to perform satisfactorily.

A. The non-linear OSNR

Even though the so-called non-linear OSNR is not strictly a part of the GN-model, it is the key tool through which the GN-model is put to use. The NL-OSNR is written as:

$$\mathrm{OSNR_{NL}} = \frac{P_{\mathrm{ch}}}{P_{\mathrm{ASE}} + P_{\mathrm{NLI}}} \tag{1}$$

where P_{ch} is the power of the channel under test (CUT). P_{ASE} is the power of ASE noise and P_{NLI} is the power of non-linearity 'noise', which we call non-linear-interference (NLI), both assessed at the output of a band-pass filter matched to the CUT signal. The assumption is that BER can be estimated by replacing the conventional OSNR, in the customary BER formulas for each format, with the NL-OSNR of Eq. (1). Note that this assumption is an approximation. In Sects. IV and V-A we will come back to this issue[2].

To obtain the NL-OSNR, the quantity P_{NLI} must be estimated. This in turn requires the knowledge of $G_{\mathrm{NLI}}(f)$, the power spectral density (PSD) of NLI. From it, P_{NLI} can be found through a formula that takes into account the actual shape of the Rx matched filter. We will not go into the details, which can be found in [1], Sect. IV. However, if the CUT makes use of pulses whose Fourier transform is root-raised-cosine, and the roll-off is small, the following approximation

[2]Throughout the paper, we will in fact use the modified formula Eq. (22) rather then Eq. (1), to estimate MR. The difference between the two formulas is discussed in Sect. V-A and it would be premature to discuss it here. It is anyway non-negligible only at low operating OSNRs, namely less than 10 dB. Sect. IV looks instead at possible inaccuracy in BER estimation through Eq. (1) related to non-linear phase and polarization noise.

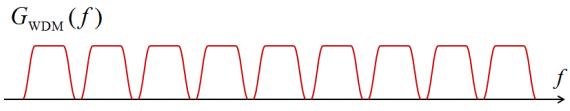

Fig. 3. A possible instance of the WDM signal power spectrum $G_{\mathrm{NLI}}(f)$, which appears in the GN-model reference formula Eq. (3).

is quite accurate:

$$P_{\mathrm{NLI}} \approx \int_{-R_s/2}^{R_s/2} G_{\mathrm{NLI}}(f)\,\mathrm{d}f \tag{2}$$

where $f{=}0$ coincides with the center frequency of the CUT. In the following, we will always look at low-roll-off systems (set to 0.05) and hence we will make use of Eq. (2).

From Eq. (2), it is clear that the primary quantity that the GN-model must provide is therefore $G_{\mathrm{NLI}}(f)$.

B. The GN-model equations

As discussed previously, by applying a first-order perturbation approach towards resolving the Manakov (non-PMD) equation, and using the signal-Gaussianity assumption, the GN-model expression of $G_{\mathrm{NLI}}(f)$, often called the GN-model reference formula, or GNRF, can be found as:

$$\begin{aligned} G_{\mathrm{NLI}}(f) = \tfrac{16}{27} \int_{-\infty}^{\infty}\int_{-\infty}^{\infty} G_{\mathrm{WDM}}(f_1)\, G_{\mathrm{WDM}}(f_2) \cdot \\ \cdot\, G_{\mathrm{WDM}}(f_1+f_2-f)\, |\mu(f_1,f_2,f)|^2 \;\mathrm{d}f_1\mathrm{d}f_2 \end{aligned} \tag{3}$$

In the equation, $G_{\mathrm{WDM}}(f)$ is the WDM signal spectrum, such as shown for instance in Fig. 3. It is an always-positive 'box-like' function which poses no problem to possible numerical integration. The factor $|\mu|^2$ is the non-degenerate-FWM efficiency of the overall link, from input to output. As such, it depends on the specific link layout. For a general analytical expression of $|\mu|^2$ covering arbitrary links, see [2], Appendix A.1.2. Here we focus on the case of all identical spans, which we call 'homogenous links', with lumped amplification, under the assumption of 'transparency', i.e., that each amplifier gain exactly equals the loss of the preceding fiber span. In this case:

$$\begin{aligned} |\mu(f_1,f_2,f)|^2 = \gamma^2 L_{\mathrm{eff}}^2 \left| \tfrac{1-e^{-2\alpha L_s} e^{j4\pi^2\beta_2 L_s (f_1-f)(f_2-f)}}{1-j2\pi^2\beta_2\,\alpha^{-1}(f_1-f)(f_2-f)} \right|^2 \cdot \\ \cdot\, \tfrac{\sin^2\left(2N_s\pi^2(f_1-f)(f_2-f)\beta_2 L_s\right)}{\sin^2(2\pi^2(f_1-f)(f_2-f)\beta_2 L_s)} \end{aligned} \tag{4}$$

All symbol definitions, with indications of consistent units, are reported in Appendix B.

The factor appearing within absolute value squared physically represents a single-span FWM efficiency. It is reasonably well-behaved and it, too, does not pose major hurdles to numerical integration. The last factor, in the form of the ratio of two $\sin^2$ functions, accounts for the coherent interference of NLI produced in different spans, occurring at the receiver. It has sometimes been called the 'array factor' due to its similarity with a quantity known by this name, arising in phased-array antennas theory. Contrary to the single-span FWM efficiency factor, the array factor is extremely hard to integrate as it consists of very many sharp peaks (see [16], App. B, Fig. 21). This problem was recognized early on and approximations were sought to eliminate it.

Fiber	α, dB/km	D, ps/(nm·km)	γ, 1/(W·km)
PSCF	0.17	20.1	0.8
SMF	0.2	16.7	1.3
NZDSF	0.22	3.8	1.5

TABLE I
PARAMETERS OF THE THREE FIBER TYPES ADDRESSED IN THIS PAPER.

As discussed in [1], Sect. III-*D*, a drastic but justifiable approximation leads to replacing the entire array factor with the number of spans N_s. This approximation can also be physically interpreted as assuming that the NLI produced in different spans sums up at the Rx *in power*, or 'incoherently'. For this reason, the resulting model has been called the 'incoherent GN-model'. For a uniform and transparent link, with lumped amplification, the incoherent GN model equation for $G_{\mathrm{NLI}}(f)$ then becomes:

$$G_{\mathrm{NLI}}(f) = N_s \gamma^2 L_{\mathrm{eff}}^2 \tfrac{16}{27} \int_{-\infty}^{\infty}\int_{-\infty}^{\infty} G_{\mathrm{WDM}}(f_1) G_{\mathrm{WDM}}(f_2) \cdot \\ \cdot G_{\mathrm{WDM}}(f_1+f_2-f) \left| \tfrac{1-e^{-2\alpha L_s} e^{j4\pi^2\beta_2 L_s (f_1-f)(f_2-f)}}{1-j2\pi^2\beta_2\,\alpha^{-1}(f_1-f)(f_2-f)} \right|^2 \mathrm{d}f_1 \mathrm{d}f_2 \tag{5}$$

Clearly, with respect to the GN-model, the incoherent GN-model makes use of this further, rather drastic, approximation. On the other hand, the gain in numerical computation efficiency is very substantial.

C. Accuracy assessment

By 'accuracy assessment' we mean that we tried to ascertain whether a given NLI model predicts with sufficient accuracy the system results obtained by very accurate numerical integration of the Manakov (non-PMD) equation. Whether such equation, under certain conditions, may be itself inadequate in modeling the actual physical propagation of the signal, it is a different matter that we consider outside of the scope of this paper.

The testing of any non-linearity model should ideally be as extensive and comprehensive as possible. In this paper we tried to adhere to this principle within the obvious limitations of computation time, given that highly-accurate full-band split-step simulations are extremely time-consuming. To this effect we decided to address 5 transmission formats (PM-QPSK and PM-QAM with 8, 16, 32 and 64 points per polarization), 3 fibers (SMF, PSCF and NZDSF), three channel spacings (33.6, 37.5 and 50 GHz), and two span lengths, one length more representative of terrestrial systems (100 km) and one of submarine systems (60 km). The parameters of the three fiber types are shown[3] in Table I.

Despite the stated purpose to cover as much of the optical system 'landscape' as possible, some limitations had to be imposed to avoid excessive system configuration numerosity. Specifically, all channels in each given system configuration had the same symbol rate and the same format, in addition to the same spacing. We call such WDM signal arrangement 'uniform'. Also, in all system configurations the links were homogenous and transparent. In addition, the vast majority of our tests were conducted at 32 GBaud and with lumped amplification, though we did some targeted investigation of other symbol rates and of distributed amplification (in Sect. III-B and Sect. VI, respectively). Finally, in the 60 km span-length case, we refrained from testing PM-QPSK, due to the excessively large expected reach. Even with these restrictions, our system overall 'landscapes' encompassed 81 different system configurations, ranging from metropolitan-distance (200 km) PM-64QAM over NZDSF, to transpacific PM-QPSK over PSCF.

Another drastic limitation that needed to be imposed was on the number of simulated channels. We settled for 15, which at the time this study was performed was the maximum number permitting the overall campaign to be carried out over the set three-month target time-span, given the available computing resources. Calculations were performed with the aid of GPUs.

As the key parameter for accuracy assessment of model predictions, we decided to use the *system maximum reach* (MR). MR is arguably the bottom-line fundamental system performance indicator, in most practical situations. Therefore, we deem this choice to be consistent with our goal, stated in the introduction, to perform the study from the viewpoint of the end-users' practical need for an effective solution to their modeling requirements.

The Rx DSP structure was chosen with non-linearity model-testing in mind. We wanted the Rx to process the signal without adding any perturbing effect and therefore CD compensation and average polarization-frame recovery, as well as timing recovery, were completely *ideal and static*. *No adaptive algorithm* was used for these quantities. Note that we later introduced NL-PN and NL-PolN mitigation algorithms (see Sect. IV) for the specific purpose of discussing these non-linear effects. However, neither these nor other mitigation algorithms were used elsewhere.

MR evaluation required that a target[4] BER be set. We decided to impose BER$=4\cdot10^{-3}$, measured on the CUT, which was the center channel of the WDM comb. BER was assessed by direct error counting, based on a conventional minimum-distance hard-decision strategy. The reference constellation for decision was found as follows. The squared distance of each received symbol was computed vs. an ideal constellation. The sum of all squared distances, over the whole sequence of transmitted symbols, was then minimized vs. a rigid rotation and scaling of the ideal constellation. The best scaled and rotated ideal constellation, i.e., the one with minimum overall

[3]The chosen parameter for SMF are fairly standard. Regarding PSCF, there are now commercial products that have lower non-linearity and lower loss than indicated in Table I. However, we preferred to adopt more conservative values. As for NZDSF, there are many different types. We could only realistically look at one. We chose parameters that are similar to those of a Corning E-LEAF$^{\mathrm{TM}}$. This does not imply any judgement of superiority of this fiber vs. any other commercial NZDSF .

[4]Recently, various alternative quantities, such as mutual information (MI), generalized mutual information (GMI) or available information rate (AIR), have been proposed for optical system performance assessment. We have considered using them, too. MR could be defined, for instance, as the maximum distance still ensuring a certain target GMI (say, 3.4 bits/symbol for a PM-QPSK system), rather than a target BER. However, in the context and for the purpose of this paper, we deemed the traditional, widely-known and well-understood concept of a hard-decision BER as appropriate. At the same time, we did not see a clear specific advantage in using GMI (or the other mentioned similar quantities), within the scope of this study.

distance from the received signal, was then used as reference for hard-decision. Note that the rotation estimated as described also compensates for the static component of phase-rotation induced by the Kerr non linearity.

The estimation of MR was performed as follows. For a given launch power per channel, the simulation tool recorded the number of spans at which the target BER was exceeded by the CUT. A properly interpolated value of the *reach* in number of spans was then found, obviously comprised between the last span for which BER was below target, and that value plus one. The simulator control algorithm operated by sweeping the launch power per channel at 0.5 dB intervals, until a clear maximum of reach vs. launch power was achieved. Parabolic interpolation of the reach values vs. power was finally used to refine the final estimate of the maximum, i.e., to find the MR.

The minimum length of each simulation was 80,000 symbols, amounting to 320,000 bits for PM-QPSK, and up to 960,000 bits for PM-64QAM. Most simulations were repeated for up to five times with different seeds. The seed governed various random aspects of the simulation including, for each channel, its data sequence, its launch polarization state and its Tx laser phase-noise, whose linewidth was set to 100 kHz[5]. It also governed a random time-delay uniformly distributed between ± 1 symbol, different for each channel. At least one simulation per system configuration was run where polarization launch was perfectly aligned among channels, no delay was applied (the symbol transitions where time-aligned at launch) and no phase-noise was present. We call this the *non-randomized* instance.

The different instances of the simulations were used to check whether a different realization of the previously listed random quantities altered significantly the MR measurement. We found no instance in which the resulting MRs differed by more than $\pm 1.5\%$ vs. the average of the set, including the non-randomized instance. This means that launch delay, state of polarization and Tx phase noise[6] are largely inconsequential as to NLI generation, at least in part due to the action of uncompensated dispersion and to the fact that PM systems scramble the signal polarization effectively. As the only exception to this general result, we found a marginal sensitivity to polarization launch for PM-QPSK. Its effect could be seen only when NL-PN mitigation was applied without simultaneous NL-PolN mitigation (see Sect. IV). Such mild dependence is possibly due to the PM-QPSK format scrambling polarization only over two of the three axes of the Stokes space. On the other hand, the actual impact on MR was minimal ($\pm 2\%$), so we took the average value of the different runs and refrained from further addressing this aspect.

[5]The linewidth of the Rx LO was set to zero to avoid any penalty from the conversion of LO phase-noise into amplitude noise due to DSP electronic CD compensation at the Rx [52]. This effect occurs independently of non-linearity and would be present even in a perfectly linear link. Since our paper focuses on the modeling of non-linearity, we consider this effect outside of the scope of our study.

[6]At the Rx we performed completely ideal Tx phase-noise compensation. This means that we did not use any phase-tracking algorithm or CPE. Rather, we simply multiplied the received optical field times $\exp(-j\phi(t))$, where $\phi(t)$ was the phase-noise process generated at the Tx. We did this because we were not interested in studying the effectiveness of any actual CPE algorithm in compensating for laser phase-noise, but rather in the effect of phase-noise on NLI generation. It turned out that Tx phase noise, at the tested linewidth of 100 kHz, did not detectably alter NLI. Note that NLI has a non-linear phase-noise component, but such non-linear phase-noise component bears no relation with Tx phase-noise. It is dealt with specifically in Sect. IV.

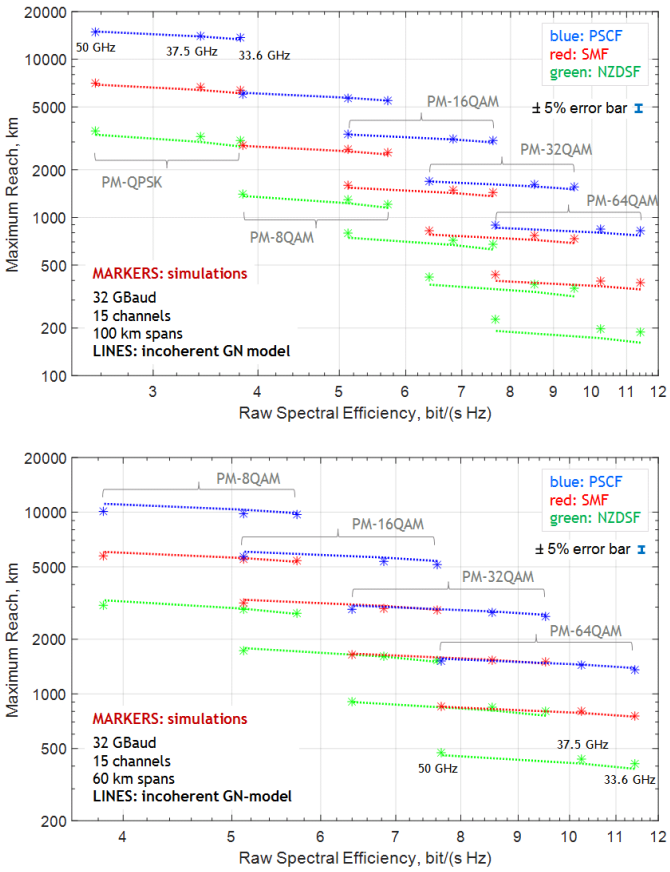

Fig. 4. Dashed lines: prediction of the system maximum reach based on the incoherent GN-model, Eq. (5), vs. each system configuration raw spectral efficiency, across the overall test 'landscapes', for span length 100 km (top) and 60 km (bottom). Markers: simulation results at 33.6, 37.5 and 50 GHz channel spacing.

All simulations were run with ASE noise entirely added at the Rx, with the exception of the simulations of Sect. V. This was done because the NLI models we considered did not include in-line ASE and we wanted to check their accuracy in this precise condition. We then introduced in-line ASE in Sect. V and separately discussed what discrepancy this did induce on MR predictions.

D. Incoherent GN-model test results

The results of our test campaign for the incoherent GN-model of Eq. (5) are shown in Fig. 4, for all the 45 and 36 systems configurations of the 'landscape' with 100 km spans (top figure) and 60 km spans (bottom figure), respectively. The dashed lines are the model predictions, whereas the markers represent simulation results. Notice in the upper right corner a reference 'error bar', or 'whisker', which amounts to $\pm 5\%$ (or 10% total) relative deviation, anywhere over the figure.

The striking feature of these plots is the good model accuracy above the 500 km MR gridline. Even below 500 km, the error exceeds 10% only in Fig. 4 (top) over NZDSF, with

PM-64QAM, at MR values of about 2 spans (200 km). Such short-reach regime was *never* intended to be handled by the GN-model, whose key premise is that the signal must have been in a thoroughly dispersed state for most of its flight along the fiber. Interestingly, the size of the errors appears to depend essentially on reach, rather than format, fiber or even span length. Above 500 km of MR, the model appears to be quite reliable, independently of all other system aspects. Below 500 km, the error grows gradually, which may make the model still usable, depending on accuracy requirements.

It should be noted that the tests of Fig. 4 do not address symbol rates lower than 32 GBaud, or dispersion lower than 3.8 ps/(nm·km). We will show in Sect. III that lower symbol rates may increase the error substantially. A safe threshold can be considered 25 GBaud. As for dispersion, we have not addressed in this study lower values than 3.8 ps/(nm·km), i.e., the NZDSF fiber of Table I. It should be conservatively assumed that near zero-dispersion regimes *cannot* be dealt with by the GN-model and should not be closely approached.

E. Closed-form incoherent GN-model test results

Though relatively simple, Eq. (5) still requires a double numerical integration. However, with the assumption of a uniform WDM signal, Eq. (5) can be integrated analytically with some further minor approximations, to yield the following closed-form expression for the overall P_{NLI} ([16], App. G):

$$P_{\mathrm{NLI}} = N_s \frac{16}{27} \frac{\gamma^2 L_{\mathrm{eff}}^2 P_{\mathrm{ch}}^3}{\pi \left|\beta_2\right| \alpha R^2} \operatorname{asinh}\left(\frac{\pi^2}{2\alpha} \left|\beta_2\right| R^2 \left[N_{\mathrm{ch}}^2\right]^{\frac{R_s}{\Delta f}} \right) \quad (6)$$

This remarkably simple closed-form formula reduces model complexity to virtually zero. It also provides a clearly readable dependence of NLI on the key system parameters. On the other hand, after so many stages of cascaded approximations, it is conceivable that its accuracy may have degraded, so that it needs to be carefully assessed.

Fig. 5 is analogous to Fig. 4, with lines now representing the MR estimate based on Eq. (6). Differences with Fig. 4 are minimal in the 100 km span picture. In the 60 km span picture, there is a small increase of error for the PSCF case. This has no relation with the basic features of the GN-model. It is due to one specific further approximation which is necessary to obtain a closed-form solution of Eq. (5) (see [16], App. F). Such approximation is valid provided that span loss is not too small, with a threshold of about 10 dB. In the case of 60 km PSCF spans, loss is 10.2 dB and this is the cause of the difference with respect to the numerical integration results of Fig. 4 (bottom). Overall, the MR error is still quite contained throughout the plot, including PSCF. Given its simplicity, the effectiveness of Eq. (6) in modeling non-linearity for the broad variety of systems of the test landscapes, spanning almost two orders of magnitude in MR, as well as spectral efficiencies from 2.5 to 11.5 bit/(s·Hz), is in our opinion quite remarkable.

As mentioned, Eq. (6) assumes uniform, transparent and homogenous systems. These three assumptions can *all* be removed while still obtaining an incoherent GN-model fully closed-form formula (Eq. (41) in [1], Sect. VI-*D*), based on the same type of approximations as those leading to Eq. (6).

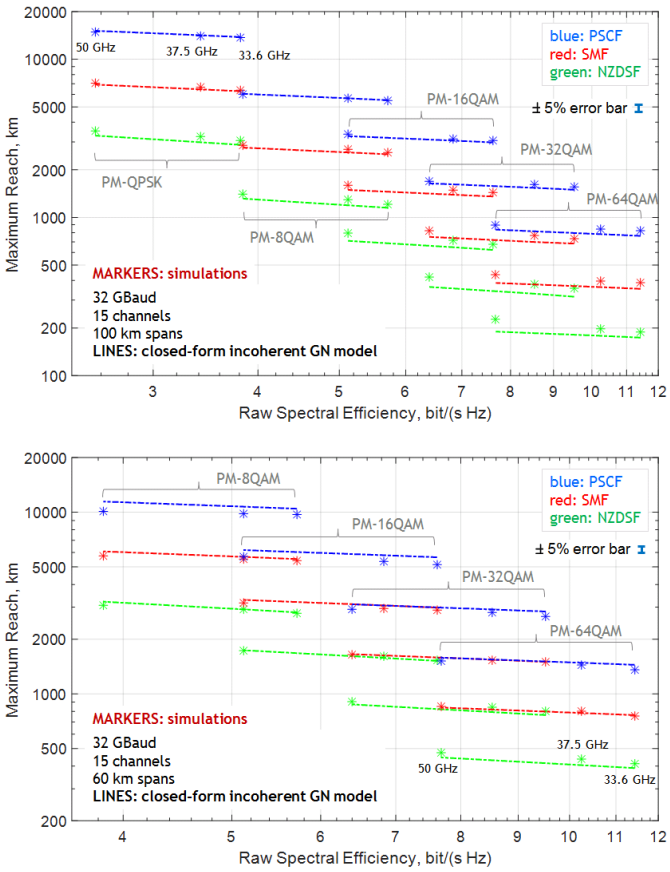

Fig. 5. Thick dashed-dotted lines: prediction of the system maximum reach based on the closed-form formula for the incoherent GN-model, Eq. (6), vs. each system configuration raw spectral efficiency, across the overall test 'landscapes', for span length 100 km (top) and 60 km (bottom). Markers: simulation results at 33.6, 37.5 and 50 GHz channel spacing.

Such general-purpose formula provides a fast-performance assessment tool which can be very useful in a number of practical applications. It is currently being used in the real-time physical-layer-aware control-plane of the commercial WDM networks of a major equipment vendor. We could not realistically test here such formula, because meaningful testing would require generating hundreds of non-uniform and non-homogenous system test configurations. Extensive experimental testing has however been done by the equipment vendor prior to commercial deployment, partially reported on in [17], [18]

It should nonetheless be remembered that these closed-form formulas inherit all the limitations intrinsic to the incoherent GN-model, listed at the end of Sect. II-D. In addition, as mentioned, span loss must be greater than 10 dB. Also, they do not account for the further effects discussed in Sects. IV-VI, which may be significant in certain system configurations.

F. Comments on the incoherent GN-model

The performance of the incoherent GN model appears remarkably good, despite the many approximations that it involves. It has been argued that its accuracy is partly due to a fortuitous error cancellation circumstance. Indeed, an error

cancellation does occur (see [1] Sect. V-*D*), but it can also be argued that this is not enough by itself to account for the incoherent GN-model overall good predictive performance. Recently, results obtained in the context of the more accurate EGN-model have provided some further justification for it. Specifically, in [23] it was analytically shown that the NLI power from inter-channel effects, which tend to dominate over single-channel effects as the number of channels grow, asymptotically accumulates *linearly* in the number of spans. This growth law is the same as that of incoherent accumulation. Hence, the incoherent GN-model mimics the correct asymptotic accumulation law of inter-channel NLI, and this contributes substantially to its generally good MR prediction performance.

G. Limitations of the GN-model

As explained in Sect. II-B, the incoherent GN-model is obtained from Eq. (5) by replacing the 'array factor' with simply N_s. It would then stand to reason that by rolling back such approximation, i.e., by re-instating the array factor, more accurate results would be found than those delivered by the incoherent GN-model.

However, this is not the case. As it can be seen by comparing Fig. 4 with Fig. 6, the GN-model performs somewhat worse than the incoherent GN-model. In particular, a fairly uniform underestimation of MR can be seen, across all system configurations[7].

This counterintuitive behavior of the GN-model vs. the incoherent GN-model was observed as early as 2011. It was then soon realized that, in order to investigate it, a better 'probe' than MR was needed. The reason why MR, while being the key system performance indicator, is not well suited for fundamental modeling studies, is twofold. First, MR is rather insensitive to NLI estimation errors. In particular, the relation between a relative deviation in P_{NLI} estimation (in dB) and the resulting relative deviation in MR estimation (in dB) is approximately given by (see [1], Sect. IV-*A*):

$$\Delta \mathrm{MR}_{\mathrm{dB}} \approx -\frac{1}{3}\Delta P_{\mathrm{NLI,dB}} \tag{7}$$

This means that an error of 1 dB in the estimation of P_{NLI} leads to only 1/3 dB error in MR estimation, or just 8%. This dampening of errors is good from a practical end-user viewpoint, because it allows simple approximate models to still deliver fairly good MR estimates. On the other hand, it shows that MR is not a 'sensitive enough' probe for fundamental modeling studies.

Besides this aspect, and perhaps more importantly, MR of course provides model accuracy information at *maximum reach*. It does not furnish any information as to the accuracy of P_{NLI} estimation along the link, which could instead provide clues as to the inner workings and potential problems of a model. A better probe for NLI modeling studies is the quantity $P_{\mathrm{NLI}}(n_s)$ itself, that is the amount of NLI power present after each span. The earliest study using this quantity was [19], where the normalization:

$$\tilde{P}_{\mathrm{NLI}} = P_{\mathrm{NLI}}/P_{\mathrm{ch}}^3 \tag{8}$$

was used to make the quantity launch-power independent[8]. The results are shown in Fig. 7. While there is substantial convergence of the simulated result (red solid curve) towards the GN-model curve (dashed line), a residual gap is present even at 50 spans into the link. The incoherent GN-model (dash-dotted line) has a better convergence, despite being a more approximate model, for the reasons discussed earlier in Sect. II-F.

Overall, Fig. 7 shows that the GN-model, either coherent or incoherent, has fundamental limitations. Also, besides the problems evidenced in Fig. 7, further limitations affect it. In particular, the GN-model loses accuracy at low symbol rates, as we shall see in Sect. III-B. It does not allow to assess some finer effects of format-dependence on NLI (see next section).

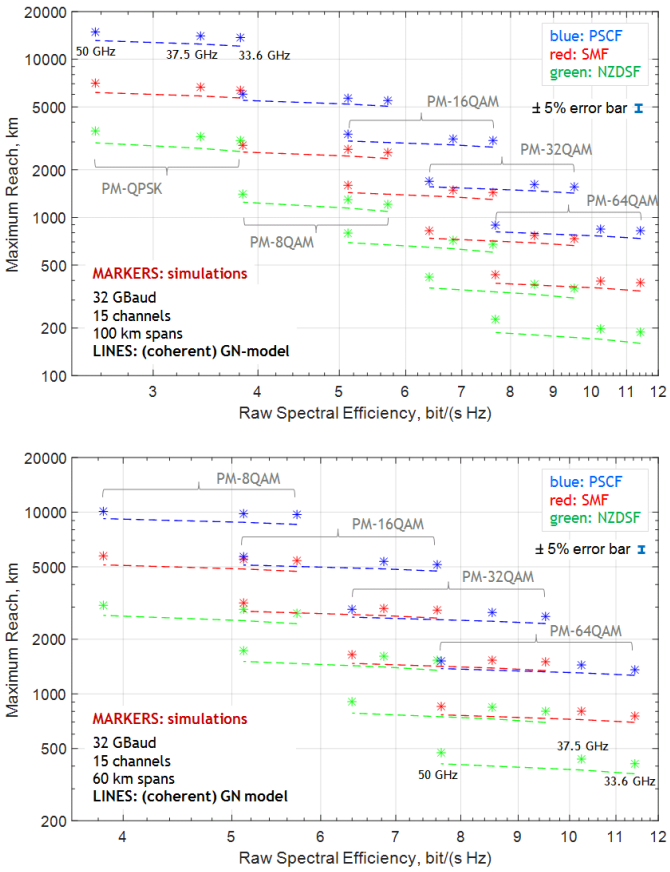

Fig. 6. Dashed lines: prediction of the system maximum reach based on the (coherent) GN-model, Eqs. (3)-(4), vs. each system configuration raw spectral efficiency, across the overall test 'landscapes', for span length 100 km. Markers: simulation results at 33.6, 37.5 and 50 GHz channel spacing.

[7]It can be shown (see Sect. III) that the GN-model provides *an upper bound* to NLI power for all PM-QAM systems (including PM-QPSK). In this sense it is a 'conservative' model, as it cannot overestimate reach. On the other hand, the results in Fig. 6 are clearly not entirely satisfactory.

[8]Both the GN and EGN models, as well as many other models, agree that the amount of NLI power on the CUT grows as the launch power per channel, cube. Hence, dividing the NLI power by P_{ch}^3 provides a power-independent estimate of the system non-linearity. This has been verified by computer simulations, and is accurate at least as long as the signal itself does not get depleted by conversion into NLI. See Sect. V for a discussion on signal depletion.

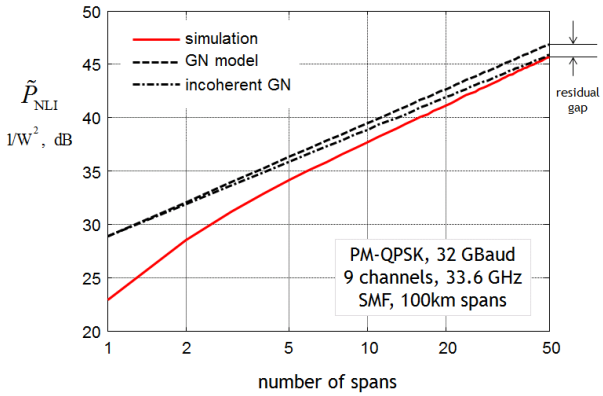

Fig. 7. Accumulated NLI power vs. the number of spans traveled into the link. The quantity $\tilde{P}_{\mathrm{NLI}}$ is normalized vs. launch power as shown in Eq. 8.

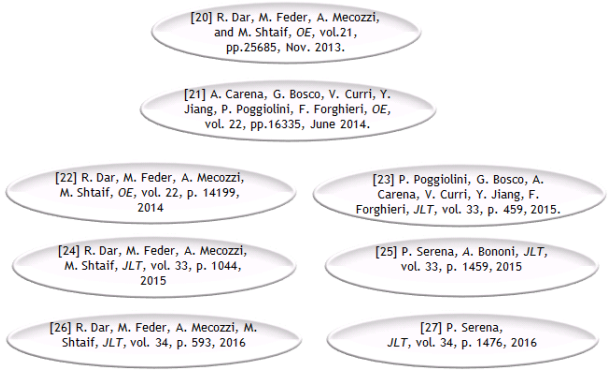

Fig. 8. The main EGN-model-related papers, from oldest at the top to most recent at the bottom.

It does not handle well NL-PN mitigation (see Sect. IV-A). A more sophisticated model would clearly be desirable for high-accuracy investigations and perhaps to support research into non-conventional systems.

III. The EGN-model

Most of the listed limitations of the GN-model originate from the signal Gaussianity assumption. Removing such assumption then appears to be a necessary step to take. This was first proposed in [20]. Put it simply, the signal Gaussianity assumption implies that only the 2^{nd} moment of the launched signal be taken into account in the model calculations. Removing the Gaussianity assumption requires taking into account the 4^{th} moment of the signal, for XPM and FWM, and both the 4^{th} and 6^{th} signal moments for SPM.

In [20] such extension was performed for the XPM contribution to NLI. In [21] it was done for the FWM and SPM contributions. These two papers contain the complete initial derivation of the so-called enhanced GN-model, or EGN-model. Several EGN-model follow-up and related publications have since appeared. A diagram of the main EGN-model-related papers is shown in Fig. 8.

The EGN model formulas are much more complex than those of the GN-model. To the best of our knowledge, the most complete and encompassing version of such formulas is currently reported in [2]. A somewhat less general version can be found in [21]. We will refrain from providing them here in full, but we highlight one specific feature of theirs.

As was the case for the GN-model, the primary goal of the EGN-model is that of providing an expression for the NLI PSD, $G_{\mathrm{NLI}}(f)$. According to the EGN-model, it can be written as:

$$G_{\mathrm{NLI}}^{\mathrm{EGN}}(f) = G_{\mathrm{NLI}}^{\mathrm{GN}}(f) - G_{\mathrm{NLI}}^{\mathrm{corr}}(f) \tag{9}$$

where $G_{\mathrm{NLI}}^{\mathrm{GN}}(f)$ is the result of the GN-model calculation and $G_{\mathrm{NLI}}^{\mathrm{corr}}(f)$ is a 'correction' term. The latter is intentionally presented with a minus sign, to stress the fact that the EGN-model correction typically *decreases* NLI. In fact, it *always* decreases NLI if PM-QAM signals are assumed[9]. Interestingly, if the signal constellation is Gaussian, then $G_{\mathrm{NLI}}^{\mathrm{corr}}(f) = 0$, that is, $G_{\mathrm{NLI}}^{\mathrm{EGN}}(f) = G_{\mathrm{NLI}}^{\mathrm{GN}}(f)$.

In the next section we are going to extensively assess the merit of the EGN-model as far as accuracy is concerned. A discussion of its accuracy vs. complexity balance is dealt with later.

A. EGN-model test results

The testing methodology was the same as used for the GN-model, over the same 'landscapes' of system configurations. The results are shown in Fig. 9. It is immediately seen that an excellent correspondence between EGN-model predictions and simulation results is found throughout the entire landscapes. The agreement is truly remarkable, given that the calculations involved in obtaining the two MR estimates, the simulative and the EGN one, are completely different in formulas and algorithms, and involve several trillions of FLOPS each. Yet, their final output agrees to within less than 3%, from 200 km to nearly 16,000.

A very good performance is now also obtained in reproducing the much more sensitive $\tilde{P}_{\mathrm{NLI}}$ indicator. Fig. 10 is analogous to Fig. 7, with the addition of the EGN estimation (green dashed curve) and the removal of the incoherent GN-model curve for clarity. From 2 to 50 spans the coincidence between the simulated and EGN-estimated $\tilde{P}_{\mathrm{NLI}}$ is almost flawless[10]. Many more similar detailed comparisons between simulation and EGN estimates of $\tilde{P}_{\mathrm{NLI}}$ can be found in [23], all indicating excellent agreement.

B. Low symbol rates

We mentioned earlier that one of the weaknesses of the GN-model is its poor performance at low symbol rates. The circumstance can be intuitively explained based on the fact that the GN-model requires a thoroughly dispersed signal

[9]It is possible to conceive signal constellations for which $G_{\mathrm{NLI}}^{\mathrm{corr}}(f)$ actually *increases* NLI vs. the GN-model contribution alone. This occurs when the so-called 'excess kurtosis' [28] of the constellation is greater than zero. However, to the best of our knowledge, no constellation in practical use has this feature.

[10]The slight divergence at span 1 can tentatively be explained as follows. The EGN model provides a value of $\tilde{P}_{\mathrm{NLI}}$ which is the average over all sampling instants, i.e., a stationarized estimate of $\tilde{P}_{\mathrm{NLI}}$. Dispersion does induce NLI first-order stationarization rather quickly, but not after just one span. So the simulative estimate (which is performed at one sample per symbol) may still be affected by non-stationary features. We propose this explanation as tentative, leaving its confirmation for future investigation.

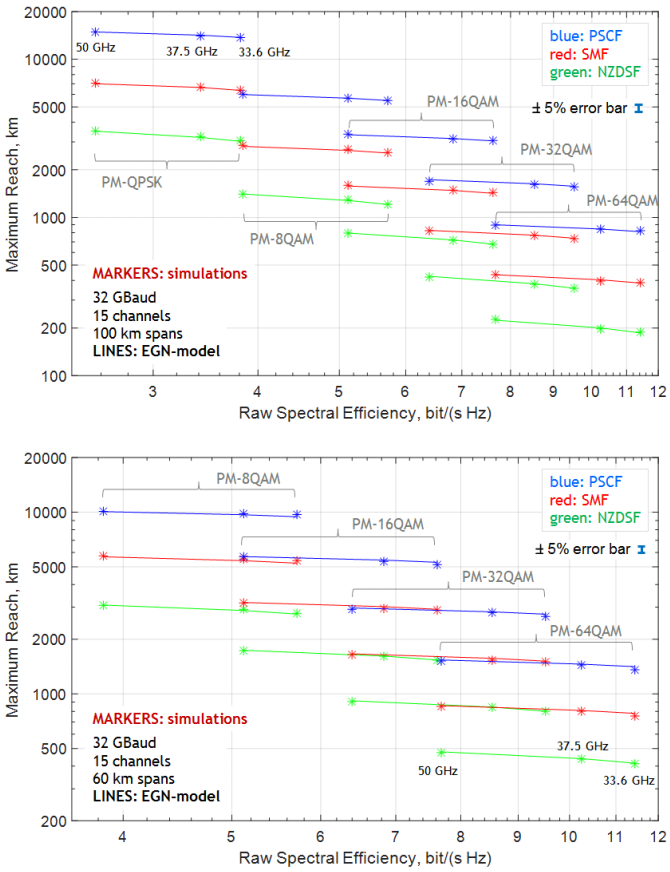

Fig. 9. Solid lines: prediction of the system maximum reach based on the EGN-model, vs. each system configuration raw spectral efficiency, across the overall test 'landscapes', for span length 100 km (top) and 60 km (bottom). Markers: simulation results at 33.6, 37.5 and 50 GHz channel spacing.

to work properly[11], which is a necessary (though not sufficient) condition for the signal Gaussianity approximation to work well-enough. The EGN-model does away with the signal Gaussianity approximation and it could therefore be conjectured to perform well even at low symbol rates, over little dispersed signals.

Before testing such conjecture, we would like to point out that accuracy at low symbol rates may seem essentially an academic topic of no practical importance since, if anything, symbol rates are steadily going up in all segments of optical communications. In particular, following recent press releases and announcements by all major vendors, the current 32 GBaud industry standard appears to be destined to be soon superseded by new systems operating at up to 64 GBaud, or even higher.

However, somewhat unexpectedly, higher symbol rates appear to carry some intrinsic non-linearity penalty vs. lower rates. Such penalty may be substantial in certain scenarios. This has led to the proposal of generating new higher-symbol-

[11]Reducing the symbol rate quickly sterilizes the effect of dispersion and invalidates this fundamental premise. As an example, the symbols of a 2.5 GBaud signal are so little dispersed that they can still be received at about 1000 km of SMF without any optical or electrical dispersion compensation, whereas at the same distance the symbols of a 32 GBaud signal have spread out over more than 100 symbol times.

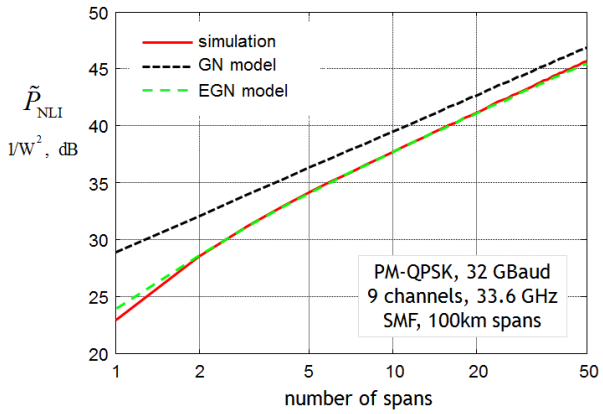

Fig. 10. Accumulated NLI power vs. the number of spans traveled into the link. The quantity $\tilde{P}_{\mathrm{NLI}}$ is normalized vs. launch power as shown in Eq. 8.

rate systems as a collection of DAC-generated electrical subcarriers each operating at the symbol-rate which is optimum from the viewpoint of NLI mitigation. This concept has been dubbed 'SRO', for 'symbol rate optimization'. For a comprehensive introduction and bibliography on SRO see [29].

Note that in this paper we are not interested in SRO. Rather, we want to probe the overall envelope of validity of certain non-linearity models. On the other hand, we deemed it important to point out that being able to accurately model NLI at low symbol rates is not just of academic interest, but there seems to be a possibly significant practical side to it.

To carry out the study, the per-channel symbol rate R_s was varied while all other key system features were kept fixed. Specifically, we imposed:

1) the total optical bandwidth B_{WDM}
2) the *relative* channel spacing $\delta f = \frac{\Delta f}{R_s}$

The above two fixed parameters determine the system spectral efficiency and the total (raw) bit rate, which are, respectively:

$$S = \frac{b_s}{\delta f} \tag{10}$$

$$R_{\mathrm{b,tot}} = B_{\mathrm{WDM}} \cdot S \tag{11}$$

where b_s is the number of bits per symbol. We assumed: B_{WDM} = 504 GHz, ρ = 0.05, δf =1.05 and PM-QPSK transmission (b_s = 4). The resulting spectral efficiency and total raw bit rates were S = 3.81 b/(s·Hz) and $R_{\mathrm{b,tot}}$ = 1.92 Tb/s.

As mentioned, R_s is a free parameter, with the obvious constraint that it had to split the WDM bandwidth into a number of channels, given by:

$$N_{\mathrm{ch}} = \frac{B_{\mathrm{WDM}}}{(1+\rho)\, R_s} \tag{12}$$

which had to be an *integer*. Note that if the value R_s = 32 GBaud is chosen, then Eq (12) yields exactly N_{ch}=15 channels and, in that case, the system set-up coincides with the one used in the 'landscapes', such as Fig. 9, to obtain the data points for PM-QPSK at 33.6 GHz channel spacing.

At the link output we measured the NLI power P_{NLI} falling on the center channel of the WDM comb (the CUT). However, simply comparing P_{NLI} across systems that use different symbol rates does not immediately provide information regarding

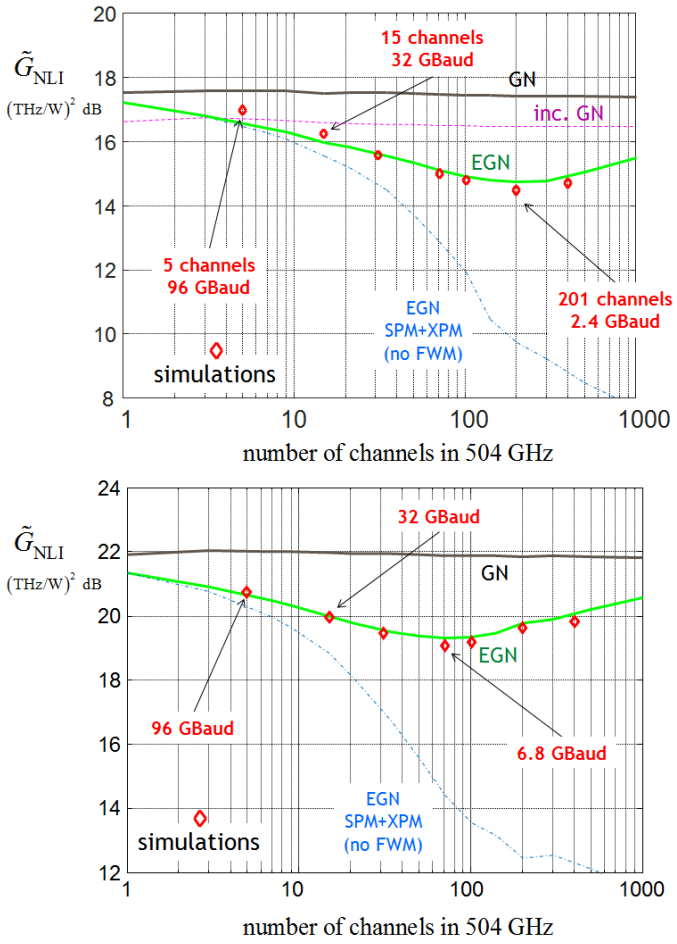

Fig. 11. Normalized average NLI noise power spectral density $\tilde{G}_{\rm NLI}$ over the center channel, vs. the number of channels in a *fixed* total WDM bandwidth of 504 GHz. PM-QPSK modulation, quasi-Nyquist: roll-off 0.05, spacing 1.05 times the symbol rate. NLI is measured at 50 spans of SMF (top) or 30 spans of NZDSF (bottom). Lines: calculations using the models indicated in figure. Markers: simulations.

their relative MR performance. We therefore derived from $P_{\rm NLI}$ a suitably normalized quantity which we called $\tilde{G}_{\rm NLI}$:

$$\tilde{G}_{\rm NLI} = \frac{P_{\rm NLI}}{R_s\, G_{\rm ch}^3} \tag{13}$$

where $G_{\rm ch}$ is the launched signal PSD measured at the raised-cosine spectrum flat-top of anyone of the launched channels, assuming as usual a uniform WDM signal. $\tilde{G}_{\rm NLI}$ can be viewed as the average value of $G_{\rm NLI}(f)$ impinging on the CUT, normalized versus the cube of $G_{\rm ch}$.

The key feature of $\tilde{G}_{\rm NLI}$ is the following: the *same value* of $\tilde{G}_{\rm NLI}$ among systems using different symbol rates means that they can potentially achieve the *same maximum reach*. This makes $\tilde{G}_{\rm NLI}$ very convenient for performance comparison across different symbol rates. Fig. 11 plots the simulation results for $\tilde{G}_{\rm NLI}$ as markers, for SMF, measured at 50 spans (top), and for NZDSF, measured at 30 spans (bottom), vs. the number of channels in which the fixed $B_{\rm WDM}$ optical bandwidth is split up. The results clearly show that $\tilde{G}_{\rm NLI}$ is *not* constant and actually has a minimum at about 2.4 GBaud and 6.4 GBaud, respectively. For an approximate analytical formula of the optimum symbol rate, see [29].

Regarding the GN-models (coherent and incoherent), they both fail to capture the decrease of $\tilde{G}_{\rm NLI}$ as the symbol rate goes down. Over SMF (Fig. 11 (top)), the incoherent GN-model (dashed line) does run quite close to the simulations in the 32-to-96 GBaud range. However, it is almost 2 dB above the $\tilde{G}_{\rm NLI}$ level at the optimum symbol rate. The GN-model is even further away. The EGN-model instead follows the simulations quite closely throughout the tested interval, with both fibers. It predicts very accurately the optimum symbol rate and the related $\tilde{G}_{\rm NLI}$ value.

We have added a further curve, that of the EGN model without the FWM contribution, because FWM is often neglected in modeling papers, on the basis that it is negligible at high symbol rates. The plots show that indeed neglecting FWM returns accurate-enough results at high symbol rates, but that such approximation cannot be trusted at low symbol rates. In particular, neglecting FWM does not produce any minimum of $\tilde{G}_{\rm NLI}$, since the no-FWM curve steadily wanes while going to lower and lower symbol rates.

More plots similar to Fig. 11, as well as actual MR simulative tests verifying the NLI mitigation obtained by optimizing the symbol rate, can be found in [29]. In conclusion, the EGN-model appears to be quite reliable at any symbol rate, even very low ones for which the signal is essentially undispersed. It can therefore be used to study multi-subcarrier system and in particular it can be used for SRO assessment.

As a final comment on this topic, it is interesting to see in Fig. 11 that the GN-model accuracy improves again towards ultra-low symbol rates (less than 1 GBaud), typical of OFDM systems. The reason is that OFDM signals tend to intrinsically take on a jointly-Gaussian overall distribution, as they are split into a very large number of independent subcarriers.

C. EGN-model closed-form approximations

The excellent accuracy of the EGN model, verified in the previous sections, is obtained at the cost of a much greater analytical and computational complexity than the GN-model[12]. It would therefore be important that some simplified and ideally closed-form approximations be available, which still retained the key features of the EGN model. This would be particularly helpful for instance for complex network optimization studies, where many model evaluations are needed to achieve even a single result.

In [23] a first step towards this goal was taken, by identifying a closed-form approximation to the *correction term* $G_{\rm NLI}^{\rm corr}(f)$ in Eq. (9), valid asymptotically in the number of spans traversed. That approximation however did not address SPM and was limited to uniform WDM signals. In [2], SPM

[12]The EGN model contains the GN-model term and a 'correction term' (see Eq. (9)). The correction term actually consists of 8 distinct terms, 1 for SPM, 1 for XPM and 6 for FWM. Each of these terms consists of one or more quadruple integrals. While it can be shown that each of these many quadruple integrals can always be rearranged so that its complexity is that of a double integral, the overall correction term $G_{\rm NLI}^{\rm corr}(f)$ is undoubtedly challenging to evaluate, and by far the leading source of the computational complexity of the EGN-model.

format	Φ
PM-BPSK	1
PM-QPSK	1
PM-8QAM	2/3
PM-16QAM	17/25
PM-32QAM	69/100
PM-64QAM	13/21
PM-∞-QAM	3/5
PM-Gaussian	0

TABLE II
VALUES OF THE Φ PARAMETER.

was factored in and a more general form capable of handling arbitrary WDM combs was provided:

$$G_{\mathrm{NLI}}^{\mathrm{corr}}(f) \approx \underrightarrow{G}_{\mathrm{NLI}}^{\mathrm{corr}} = \frac{40}{81}\frac{\gamma^2 P_m N_s \bar{L}_{\mathrm{eff}}^2}{R_m \pi \beta_2 \bar{L}_s} \cdot \left(\sum_{\substack{n=1 \\ n\neq m}}^{N_{\mathrm{ch}}} \Phi_n \frac{P_n^2}{R_n \left| f_n - f_m \right|} + \Phi_m \frac{2P_m^2}{R_m^2} \right) \quad (14)$$

The arrow underneath $\underrightarrow{G}_{\mathrm{NLI}}^{\mathrm{corr}}$ is a reminder of the asymptotic behavior of the approximation. The symbols P_n, R_n and f_n are the launch power, symbol rate and center frequency of the n-th channel. The m-th channel is the CUT. The constant Φ_n depends on the modulation format of the channel. Its values for some of the main transmission formats are shown in Table II.

Notice that $\underrightarrow{G}_{\mathrm{NLI}}^{\mathrm{corr}}$ does not depend on frequency. It is assumed to be (approximately) constant over the band $[f_m - R_s/2, f_m + R_s/2]$, where f_m is the CUT center frequency, and zero outside of such band. Also, the formula assumes a homogenous and transparent link with lumped amplification. However, if the spans are not the same length, the average span length $\bar{L}_s$ and the average span effective length $\bar{L}_{\mathrm{eff}}$ can be used. This further approximation works well for links having all individual span lengths within $\pm 15\%$ of the average. If the WDM signal is uniform, and the CUT is the center channel, then the formula can be simplified (without further approximations) as:

$$\underrightarrow{G}_{\mathrm{NLI}}^{\mathrm{corr}} = \frac{80}{81}\Phi \frac{\gamma^2 \bar{L}_{\mathrm{eff}}^2 P_{\mathrm{ch}}^3 N_s}{R^2 \Delta f \pi \beta_2 \bar{L}_s} \left[\mathrm{HN}\left(\left[N_{\mathrm{ch}} - 1 \right] / 2 \right) + \frac{\Delta f}{R} \right] \quad (15)$$

where HN stands for harmonic number series, defined as: $\mathrm{HN}(N) = \sum_{n=1}^{N} (1/n)$.

We tested the simple formula above in the usual landscape of system configurations. We approximated Eq. (9) as:

$$G_{\mathrm{NLI}}^{\mathrm{EGN}}(f) \approx G_{\mathrm{NLI}}^{\mathrm{GN}}(f) - \underrightarrow{G}_{\mathrm{NLI}}^{\mathrm{corr}} \quad (16)$$

to assess the NLI PSD for the CUT and otherwise proceeded as before. The MR results are shown in Fig. 12. Remarkably, the accuracy is excellent throughout the plots and no substantial difference can be appreciated with Fig. 9. The single exception is a very small error in the case of PM-64QAM over NZDSF in Fig. 12 (top). The reason is that, as stated, Eq. (14) is asymptotically accurate in the number of spans. At a MR of only 2 spans, convergence is not fully achieved.

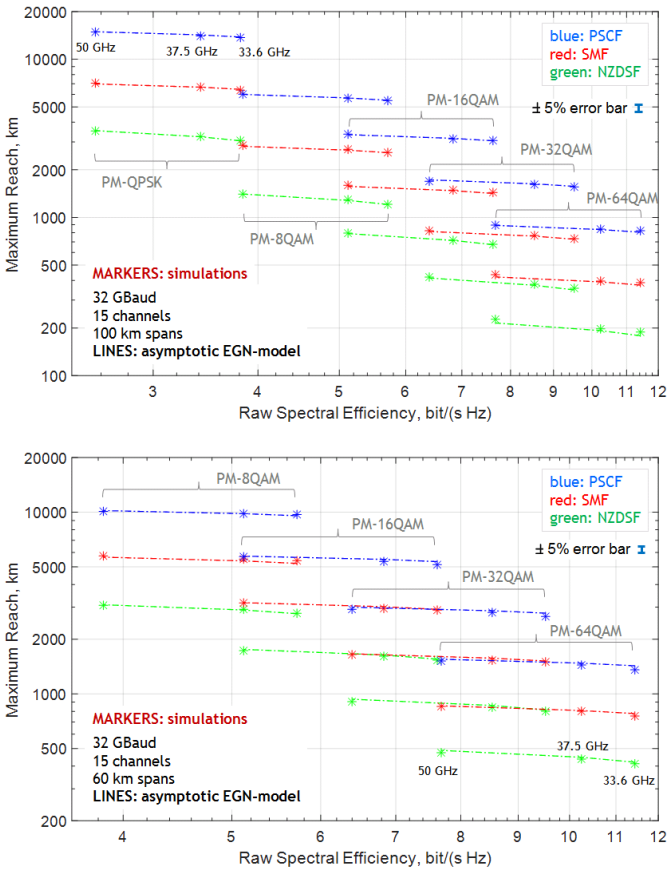

Fig. 12. Dashed-dotted lines: prediction of the system maximum reach based on the asymptotic EGN-model of Eqs. (15)-(16), vs. each system configuration raw spectral efficiency, across the overall test 'landscapes', for span length 100 km (top) and 60 km (bottom). Markers: simulation results at 33.6, 37.5 and 50 GHz channel spacing.

To gain insight into the typical behavior of the asymptotic approximation vs. the number of spans, we focus on the case of PM-QPSK over SMF, with 33.6 GHz spacing, SMF, 100 km span-length, which corresponds to one of the landscape configuration. We plot for this system $\tilde{P}_{\mathrm{NLI}}(n_s)$, in Fig. 13. The asymptotic approximation is poor for the first few spans, but it then rather quickly joins up with the simulated and EGN-model generated curves. Note that in plots like Fig. 13, drawn for higher-order formats, the spread among curves actually reduces, even at low span numbers.

The results of Fig. 12 show the potential of the asymptotic approximation to $G_{\mathrm{NLI}}^{\mathrm{corr}}(f)$. One important caveat must however be mentioned. Eq. (9) has two terms on its right hand side which may actually be comparable in absolute value, but are opposite in sign. When subtracting two quantities, the relative error on the result can exceed the relative error on either operand. In particular, we found that if the GN-model contribution $G_{\mathrm{NLI}}^{\mathrm{GN}}(f)$ and the EGN correction $G_{\mathrm{NLI}}^{\mathrm{corr}}(f)$ are *independently* approximated, then large deviations from the correct result can be incurred. Our strong recommendation is that, when using the asymptotic closed-form approximations of $G_{\mathrm{NLI}}^{\mathrm{corr}}(f)$, the GN-model term $G_{\mathrm{NLI}}^{\mathrm{GN}}(f)$ be not approximated, or otherwise a very accurate well-validated approximation be

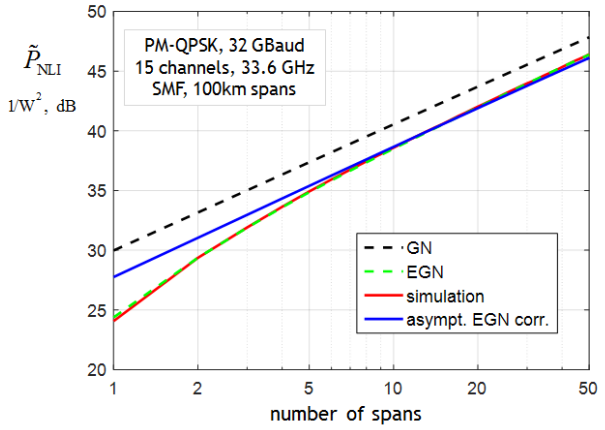

Fig. 13. Accumulated NLI power vs. the number of spans traveled into the link. The quantity $\tilde{P}_{\rm NLI}$ is normalized vs. launch power as shown in Eq. 8.

used. Note in particular that it is inappropriate to replace $G^{\rm GN}_{\rm NLI}(f)$ with the incoherent GN-model approximation discussed in Sect. II-B. We leave the interesting topic of a reliable overall closed-form approximation of Eq. (9) for future investigation. Throughout this section, when approximating Eq. (9) with Eq. (16), we have always evaluated accurately the GN-model contribution $G^{\rm GN}_{\rm NLI}(f)$.

As shown in Fig. 12, Eqs. (15)-(16) are extremely effective at 32 GBaud. The question then arises whether they retain their effectiveness at lower symbol rates. Fig. 14 represents the same quantity $\tilde{G}_{\rm NLI}$ shown in Fig. 11, vs. the number of channels into which a given optical bandwidth $B_{\rm WDM}$ is cut up. In the top plot, $B_{\rm WDM}$=504 GHz and 32 GBaud corresponds to 15 channels. In the bottom plot, $B_{\rm WDM}$=2.52 THz and 32 GBaud corresponds to 75 channels. The top plot shows that the asymptotic approximation Eqs. (15)-(16) matches the EGN-model quite well down to about 5 GBaud (100 Channels). The bottom plot shows a somewhat less accurate match, but still much better than either the GN-model, or the EGN-model neglecting FWM. As a whole, the error is rather contained down to the optimum symbol rate, which is about 2.4 GBaud in both plots. Note however that the asymptotic approximation curve does not show a minimum and therefore, to perform optimization studies, the full EGN-model must be used.

In conclusion, the closed-form correction-term asymptotic approximation Eqs. (14)-(15) greatly reduces the EGN-model complexity and is very reliable at 32 GBaud or higher. For lower symbol rates, it loses accuracy very gradually. However, it cannot be used for detailed NLI-vs.-symbol-rate optimization studies.

IV. Non-linear phase and polarization noise

Recent investigation has shown that NLI in UT systems consists of contributions that are qualitatively different [20], [22], [24], [26], [30]-[36]. Specifically, NLI can be roughly subdivided into:

- short-correlated quasi-circular noise
- long-correlated non-linear phase-noise (NL-PN)
- long-correlated non-linear polarization-noise (NL-PolN)

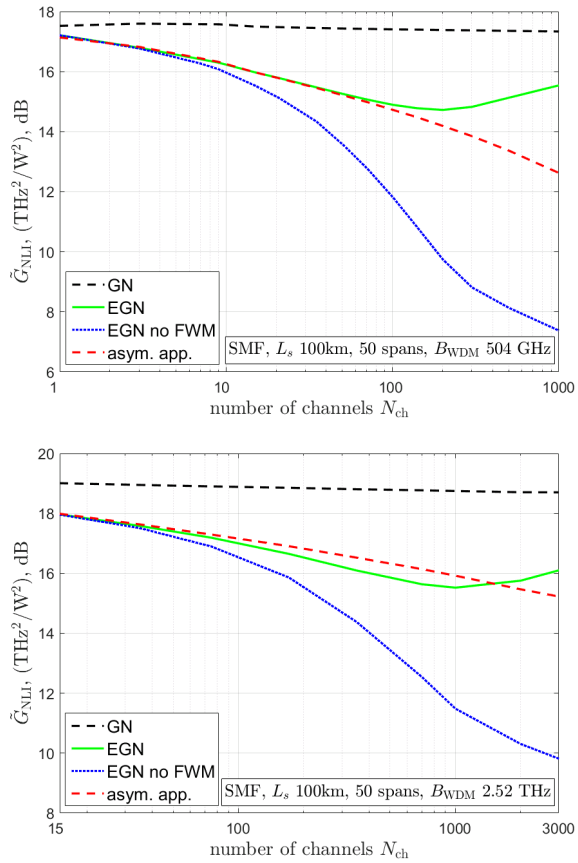

Fig. 14. Normalized average NLI noise power spectral density $\tilde{G}_{\rm NLI}$ over the center channel, vs. the number of channels $N_{\rm ch}$, for a *fixed* total WDM bandwidth of 504 GHz (top) and 2.52 THz (bottom). PM-QPSK modulation, quasi-Nyquist: roll-off 0.05, spacing 1.05 times the symbol rate. NLI is measured at 50 spans of SMF. Lines: calculations using the models indicated in figure. The label 'asym. app.' is the asymptotic EGN-model approximation of Eqs. (15)-(16).

The first paper, to the best of our knowledge, pointing out the long-correlated nature of NL-PN in UT systems, and estimating the time-length of such correlation, was [30]. Lately, experimental confirmations of the theoretical findings on NL-PN have been published, too [34], [35].

The important aspect about the said diversity among non-linear noise types is that significant portions of NL-PN and NL-PolN can ideally be removed by the Rx DSP, because of their long correlation, so that their system impact is substantially mitigated[13]. On the other hand, the EGN-model in its present form does *not* discriminate among NLI types. As a result, the EGN-model may end up overestimating the impact of NLI on a given system because it cannot account for the mitigation of NL-PN and NL-PolN.

In this section we investigate this topic, again from a very practical end-user stand-point. Our goal is to estimate the amount of inaccuracy possibly stemming from assessing MR based on the EGN-model, in the presence of NL-PN

[13]Note that some amount of long-correlated NL-PN mitigation takes place in virtually all coherent systems, even unintededly, because all receivers must have some type of CPE circuitry for carrier recovery and laser phase noise suppression.

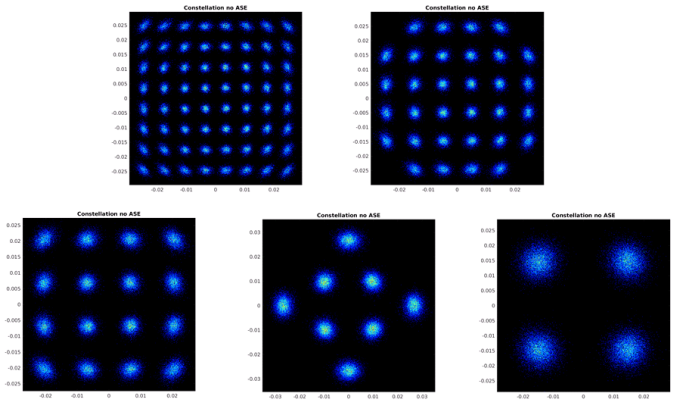

Fig. 15. Received constellations of the landscape configurations using SMF with span length 100 km and channel spacing 37.5 GHz, each at the respective maximum reach. ASE noise is not present, NLI only is shown.

and NL-PolN mitigation. We will show that in our reference 'landscape' configurations this error is modest. At any rate, we propose an effective correction that appears to mostly remove such inaccuracy and also provide some intuitive insight on the effect.

A. Non-linear phase-noise

To get some visual appreciation of the presence and typical strength of NL-PN, we show in Fig. 15 the constellations of the 'landscape' systems operating over SMF, with span length 100 km and channel spacing 37.5 GHz. ASE noise is not present, to allow appreciating the NLI disturbance alone. Tx laser phase noise is also turned off. The constellations are shown at their respective maximum reach, with optimum launch power. Some amount of NL-PN is clearly present and it is therefore important to assess the impact of its possible mitigation on the accuracy of the EGN-model MR prediction.

In particular, it would be very useful to upper-bound such impact. This requires creating a situation of maximum disagreement between the EGN-model-predicted P_{NLI} and the actual residual P_{NLI} after NL-PN mitigation. Ideally, this could be obtained by removing *all* of the long-correlated NL-PN. To try to approach this situation as much as possible, we used a CPE algorithm called 'PN-receiver', which was proposed in [36]. It is an 'idealized' algorithm because it assumes perfect knowledge of past sent symbols. To verify its effectiveness, we tested it on a case-study, selected among the 'landscape' configurations. Note that we applied the PN-receiver *separately and independently* on the two signal polarizations. This will have important implications in Sect. IV-B, to which we refer the reader for the details.

We chose PM-16QAM over PSCF with 60 km spans and 37.5 GHz channel spacing. The choice of 60 km rather than 100 km was made because a greater amount of NL-PN is produced as the span-length is shortened [22], [24]. In Fig. 16 (a) we show the received constellation at MR (about 5500 km). Again, substantial NL-PN appears to be present. To gather insight into its correlation features, we used the same procedure employed in [32] for QPSK, adapted here to

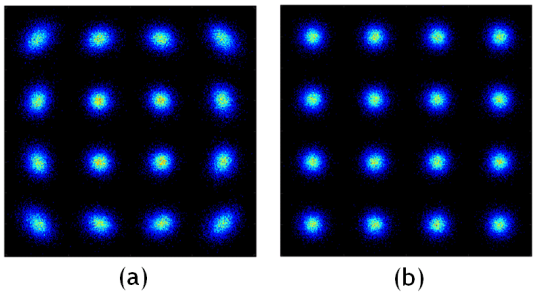

Fig. 16. Constellations of PM-16QAM over PSCF with 60 km spans and 37.5 GHz channel spacing, 15 channels, at maximum reach (about 5500 km). ASE noise and Tx laser phase-noise turned off. Non-linear phase-noise mitigation through the PN-receiver turned off (a) and on (b).

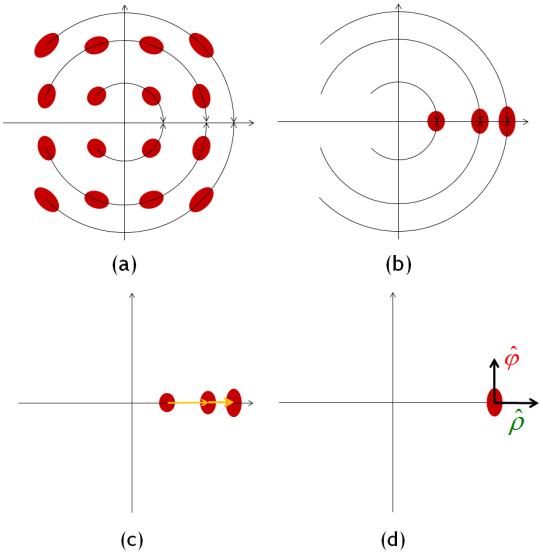

Fig. 17. Visual depiction of the constellation processing performed on 16QAM to analyze non-linear phase noise. (a) is the constellation generated by the received *noisy* symbols y_n. Each of the noisy constellation dots in (a) is rotated along the circle it lies on, till all dots merge onto three (b). The three dots are further merged onto one by translation and scaling, (c) and (d). The resulting single dot is analyzed along its tangent $\hat{\varphi}$ and radial $\hat{\rho}$ axes.

16QAM. The procedure is *pictorially* explained in Fig. 17 (see also caption). Formally, if x_k and y_k are complex numbers representing the k-th ideal transmitted symbol and the k-th noisy received symbol, respectively, then the single dot of Fig. 17 (d) is the result of the accumulation of the rotated and scaled noisy symbols q_n, which are found as $q_n = y_n/x_n$.

Note that whatever long-correlated NL-PN is present on the received constellation Fig. 16 (a), it lies tangent to the circles shown in Fig. 17 (a). After the overall processing of Fig. 17, such phase-noise turns out to be aligned with the $\hat{\varphi}$ direction in Fig. 17 (d). Mathematically, the *overall* non-linear noise (not just long-correlated NL-PN) affecting the k-th symbol along the $\hat{\varphi}$ direction, that we call $n_{\hat{\varphi}}$, can be isolated by simply taking the imaginary part of q_n, that is: $n_{\hat{\varphi}} = \mathrm{imag}\{q_n\}$. To find out whether it contains a long-correlated component, its autocovariance needs to be computed. For the study-case of Fig. 16 (a), the result is depicted in Fig. 18 (top).

The plot shows in striking clarity that two very distinct

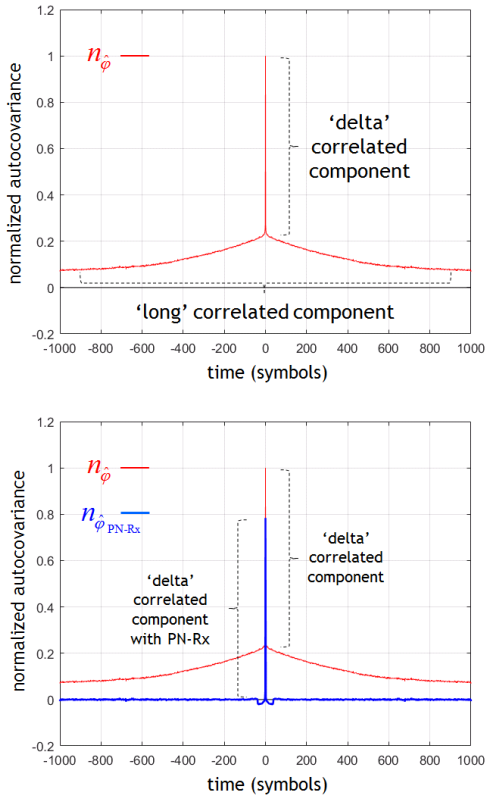

Fig. 18. Autocovariance of the tangent noise component of the single aggregated constellation point from Fig. 17 (d). The amplitude of the curves is normalized vs. the maximum for $n_{\hat{\varphi}}$. Top: without the PN-receiver. Bottom: with and without the PN-receiver. Measurement taken on simulations at maximum reach (5500 km).

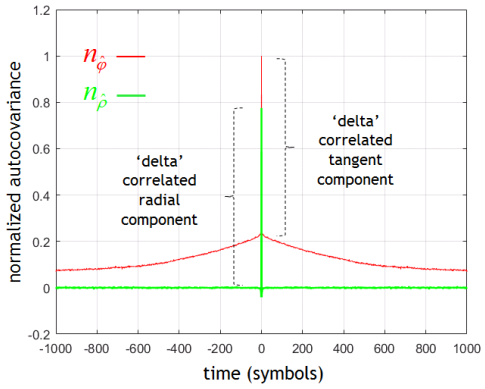

Fig. 19. Comparison of the autocovariance of the radial and tangent noise component of the single aggregated constellation point from Fig. 17 (d). The amplitude of the curves is normalized vs. the maximum for $n_{\hat{\varphi}}$. Measurement taken at maximum reach (5500 km).

kinds of noise coexist within $n_{\hat{\varphi}}$. One is delta-autocorrelated and represents almost 80% of the variance of $n_{\hat{\varphi}}$. The other kind represents slightly over 20% of the variance and produces the wide pedestal that is visible in the autocovariance. Such pedestal takes about 400 symbols to decay by 50% vs. its value near the origin, showing indeed a very long correlation on the symbol-time scale.

We then used the PN-receiver on the signal of Fig. 16 (a), obtaining a new set of received symbols which we call $\tilde{y}_n$. To such symbols we applied the same processing of Fig. 17 and then calculated again the autocovariance of the tangent noise $n_{\hat{\varphi}}$. The result is the blue solid line in Fig. 18 (bottom). The long-correlated pedestal has *completely* disappeared. The delta-correlated component is instead unchanged and its height is identical to that of the curve without PN-receiver. Note that the small undershoot near the delta is an artifact of the PN-receiver. Its impact is anyway negligible. Note also that, although difficult to appreciate on the scale of the figure, the numerical delta is indeed only one-symbol-time wide.

From the above case-study, it appears that the PN-receiver does indeed remove all the long-correlated component of the tangent noise, at least in this study case. To complete the analysis, it is however necessary to also look at the radial noise component in Fig. 17 (d), $n_{\hat{\rho}}$. Its autocovariance is shown in Fig. 19. Its remarkable feature is that the radial non-linear noise has no long-correlated component (the PN-receiver is not applied here and it would not affect $n_{\hat{\rho}}$ anyway). Note also the important aspect that the delta-correlated component of $n_{\hat{\rho}}$ has the same height as the delta-correlated component of $n_{\hat{\varphi}}$. This means that after removing long-correlated NL-PN, the noise is essentially 'circularized'. Not shown for brevity, $n_{\hat{\varphi}}$ and $n_{\hat{\rho}}$ have completely zero cross-correlation, both with and without the PN-receiver. This allows to conclude that, at least to within a good approximation, the PN-receiver removes all long-correlated NL-PN, leaving circular, delta-correlated noise on the constellations points. This now fully justifies the appearance of the simulated constellation of Fig. 16 (b).

Further interesting evidence is provided by looking at the variance of $n_{\hat{\varphi}}$ and $n_{\hat{\rho}}$, which we call $\sigma^2_{\hat{\varphi}}$ and $\sigma^2_{\hat{\rho}}$, respectively. If $\sigma^2_{\hat{\varphi}} > \sigma^2_{\hat{\rho}}$, then the 'phase-noise-like' elliptic look of the dots in Fig. 16 (a) or in Fig. 17 is found. Instead, if $\sigma^2_{\hat{\varphi}} = \sigma^2_{\hat{\rho}}$, a circular 'dot' would be seen, as in Fig. 16 (b). In Fig. 20 we plot the ratio in dB of $\sigma^2_{\hat{\varphi}}$ to $\sigma^2_{\hat{\rho}}$, which we call 'non-circularity index'. The curve without the PN-receiver shows large amounts of non-circularity throughout the link, albeit gradually declining vs. distance. With the PN-receiver the curve shows virtually perfect circularity from 1000 km onward, and already at 240 km (4 spans) the index has fallen below 0.5 dB.

We can now look at the EGN-model MR predictions over the test 'landscapes', as compared to simulations run with the PN-receiver. The results are shown in Fig. 21. The plots indicate that the PN-receiver improves performance across the board, as it should be expected, with two notable exceptions. First, PM-QPSK remains essentially unchanged. The reason is that PM-QPSK generates very little phase-noise [20] and hence, even though the little phase-noise that is there is removed, the impact of such removal is minimal. Secondly, the effect of the PN-receiver appears somewhat weaker at very low values of MR. There, it appears that NL-PN cannot entirely be removed. The reason is that for the PN-receiver to remove it, sufficiently long correlation must have developed. However, as pointed out in [30], correlation depends, among other things, on accumulated dispersion. In shorter-haul systems the signal

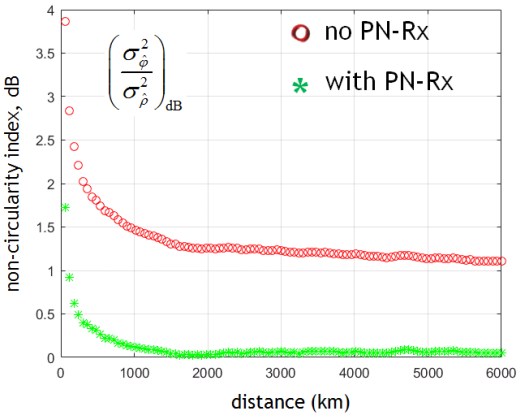

Fig. 20. Non-linear noise 'non-circularity index', defined as the ratio of the variances of non-linear noise in the tangent and radial directions to the processed constellation point shown in Fig. 17 (d). Circles: with the PN-receiver. Stars: without.

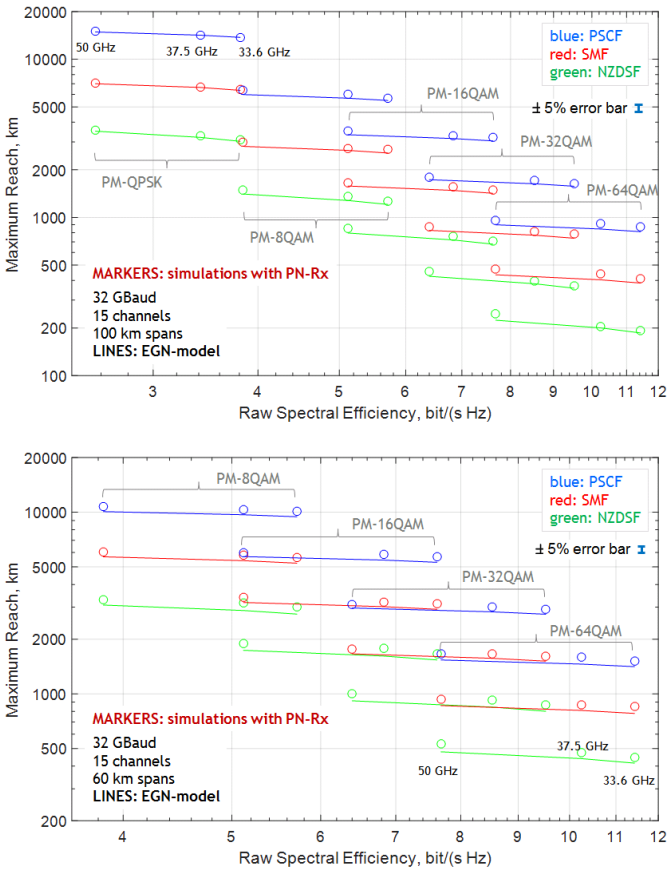

Fig. 21. Solid lines: prediction of the system maximum reach based on the EGN-model, vs. each system configuration raw spectral efficiency, across the overall test 'landscapes', for span length 100 km (top) and 60 km (bottom). Circles: simulation results with the PN-receiver (i.e., with non-linear phase noise mitigation) at 33.6, 37.5 and 50 GHz channel spacing.

does not experience enough of it.

For instance, PM-64QAM over NZDSF, 100-km spans and 37.5 or 33.6 GHz spacing, shows less improvement than other systems. In that case we found that the autocovariance of NL-PN decays by 50% in only 3 symbols, as opposed to the 400 symbols of the case-study analyzed in Fig. 18 (a). Whether a more sophisticated algorithm than the PN-receiver could better remove NL-PN there too, is beyond the scope of this paper and remains, to the best of our knowledge, an open question. From our data, it appears that a threshold of accumulated dispersion, for NL-PN to be long-correlated enough to be essentially completely removed by the PN-receiver, is about 3000 ps/nm. However, we expect that this number may vary based on operating OSNR and perhaps other system parameters.

Overall, not counting PM-QPSK, in Fig. 21 the average EGN-model MR prediction error is -5.5% in the 100 km-spans landscape and -7.6% in the 60 km-spans landscape. These errors appear relatively contained. They may or may not be problematic depending on the type of application. At any rate, we propose a phenomenological correction that adds no complexity to the EGN-model and works very well in removing the MR underestimation error shown in Fig. 21. Note that there are specific modeling approaches that allow to accurately single-out long-correlated NL-PN (see Sect. VII) at the cost of added complexity.

The correction consists of calculating NLI with the EGN-model *as if* the transmitted signal was PM-QPSK, whatever the actual PM-QAM format is. The rationale behind this correction hinges on a recently-made observation: once long-correlated NL-PN has been removed, all QAM formats tend to produce the same amount of NLI as PM-QPSK[14].

The results are shown in Fig. 22. The mean of the *absolute errors* drops to only 1.8% and 1.1%, in the 100 km and 60 km span-length landscapes, respectively. In fact, the match with simulations is essentially perfect all over the plots, with the only exception of the shortest-reach systems over NZDSF, where some modest error is visible. The reason of the slight mismatch is likely due to the already discussed short correlation of NL-PN in those systems (a few symbol times), so short that even the idealized PN-receiver cannot completely remove NL-PN. It may be conjectured that if complete NL-PN removal could be performed, then the slight mismatch would disappear. However, we leave this topic for possible future investigation.

In summary, long-correlated NL-PN *is* present in UT systems, and the EGN model actually accounts for its variance quite accurately. However, part or all of this kind of non-linear noise is removed in practical systems by the Rx CPE stage. This may cause the EGN-model-based MR prediction to somewhat overestimate the overall NLI variance, and hence underestimate the actual MR. The amount of underestimation is however rather contained. Assuming an idealized CPE such as the PN-receiver, the MR underestimation is about 5% to 8% over the test landscapes. In addition, the easy phenomenological correction of assuming PM-QPSK in the EGN-model calculations for all formats appears to yield very accurate MR predictions, provided that NL-PN is long-correlated enough for

[14]The observation and analysis of this interesting phenomenon has been reported in a specifically devoted paper [37], which also includes an experimental confirmation. The paper has been accepted for oral presentation at ECOC 2016. We refer the readers to that paper for further details.

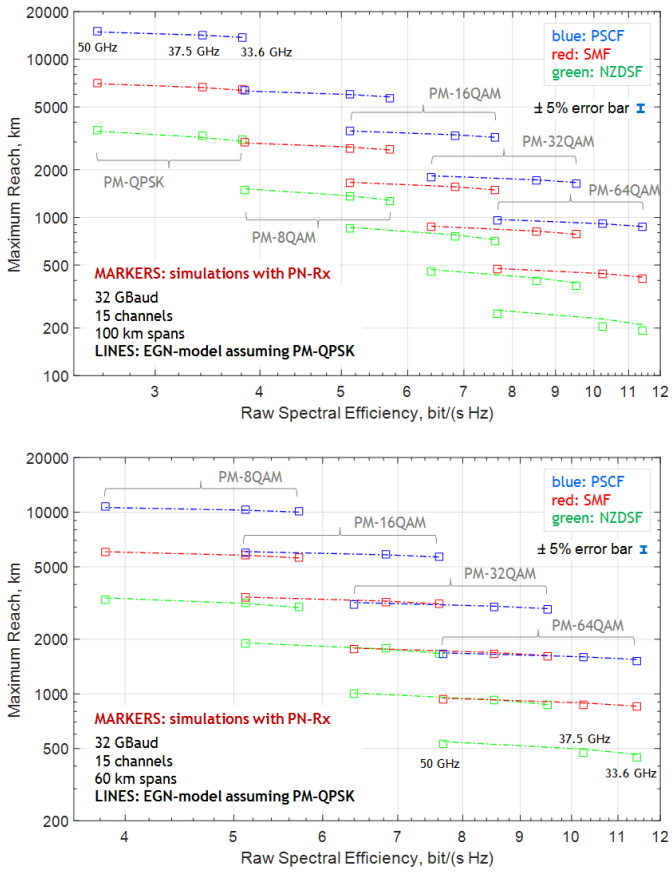

Fig. 22. Dash-dotted lines: prediction of the system maximum reach, based on the EGN-model calculated as if PM-QPSK was transmitted in all cases, vs. each system configuration raw spectral efficiency, across the overall test 'landscapes', for span length 100 km (top) and 60 km (bottom). Circles: simulation results with the PN-receiver (i.e., with non-linear phase noise mitigation) at 33.6, 37.5 and 50 GHz channel spacing.

the Rx CPE to effectively remove it. This required about 3000 ps/nm of accumulated dispersion to occur in our landscape system configurations, when using the idealized PN-Rx.

B. Non-linear polarization-noise

As mentioned, NL-PN is not the only long-correlated type of NLI which is present in WDM systems. Another type of NLI that has a long-correlated component is NL-PolN.

While NL-PN mitigation is commonplace (even unintededly because, as mentioned, all Rx's must have some type of CPE), to the best of our knowledge NL-PolN mitigation is not widely adopted. However, especially following the publication of [24], awareness of the potential removal of such NLI component has been spreading.

NL-PolN is a well-known component of Kerr-generated non-linear effects. A powerful mathematical description, in terms of the precession of each channel's Stokes vector about the resultant Stokes vector of all WDM channels together, was proposed in [38]. Such description directly implies that NL-PolN can be written as a time-varying stochastic Jones matrix of birefringence:

$$\mathbf{U}_{\mathrm{PolN}} = \begin{bmatrix} e^{j\Phi}\cos\Gamma & -e^{-j\Psi}\sin\Gamma \\ e^{j\Psi}\sin\Gamma & e^{-j\Phi}\cos\Gamma \end{bmatrix} \tag{17}$$

where the phases Φ, Ψ and Γ are random processes. These random processes have a long-correlated component which can be potentially mitigated. Under the reasonable assumption that, even at maximum reach, the angle Γ is small, we can approximate Eq. (17) and write:

$$\begin{bmatrix} s_{\hat{x},\mathrm{Rx}} \\ s_{\hat{y},\mathrm{Rx}} \end{bmatrix} = \mathbf{U}_{\mathrm{PolN}} \cdot \begin{bmatrix} s_{\hat{x}} \\ s_{\hat{y}} \end{bmatrix} \approx \begin{bmatrix} s_{\hat{x}} \cdot e^{j\Phi} - s_{\hat{y}} \cdot \Gamma \cdot e^{-j\Psi} \\ s_{\hat{y}} \cdot e^{-j\Phi} + s_{\hat{x}} \cdot \Gamma \cdot e^{j\Psi} \end{bmatrix} \tag{18}$$

where $[s_{\hat{x}} \;\; s_{\hat{y}}]^{\mathrm{T}}$ is the Jones vector of the transmitted signal and $[s_{\hat{x},\mathrm{Rx}} \;\; s_{\hat{y},\mathrm{Rx}}]^{\mathrm{T}}$ is the Jones vector of the received signal. Apart from Γ being small, Eq. (18) makes various other simplifying assumptions. One is that all conventional (linear) birefringence has been compensated for, so that $\mathbf{U}_{\mathrm{PolN}}$ is only due to non-linear effects. Secondly, we do not explicitly indicate any other non-linear disturbance, or ASE noise either, for the sake of singling out NL-PolN. Finally, without any loss of generality, we assume that in the absence of any disturbance, the two independent signal constellations are mapped exactly onto the $\hat{x}$ and $\hat{y}$ polarization.

If we concentrate on the $\hat{x}$ constellation alone, from Eq. (18) we can write:

$$s_{\hat{x},\mathrm{Rx}} \approx s_{\hat{x}} \cdot e^{j\Phi} - s_{\hat{y}} \cdot \Gamma \cdot e^{-j\Psi} \tag{19}$$

which shows that the received $\hat{x}$ constellation is corrupted by two distinct effects: one is a phase rotation, by an angle Φ, the other is crosstalk from the $\hat{y}$ constellation, whose strength is proportional to $(-\Gamma)$ and is phase-rotated by $(-\Psi)$.

So, based on Eq. (19), part of NL-PolN actually shows up as NL-PN, through Φ. The obvious question is then: how does Φ relate to the NL-PN dealt with in detail in Sect. IV-A? The answer is that NL-PN has a 'scalar' phase component, that we call Θ, and a NL-PolN-related component Φ. While Θ rotates both the $\hat{x}$ and $\hat{y}$ constellations in the same direction, Φ rotates them in *opposite* directions (see the sign inversion on Φ in Eq. (18)). In other words, the *total* NL-PN for the $\hat{x}$ constellation is $(\Theta + \Phi)$ whereas the *total* NL-PN for the $\hat{y}$ constellation is $(\Theta - \Phi)$. In Sect. IV-A, as mentioned there, *two* PN-receivers were actually used, one per constellation, which operated *independently*. This way, the respective *total* NL-PN was mitigated on each constellation, including the NL-PolN-related phase-noise component Φ. Note that if a single PN-receiver were used on the NL-PN that is in *common* between the two constellations, then only the scalar Θ component would be mitigated.

If we assume that two independent PN-receivers are used, so that both long-correlated Θ and Φ phase-noise contributions are removed, then what remains of NL-PolN is *crosstalk* from the other polarization, and Eq. (18) can be simplified as:

$$\begin{bmatrix} s_{\hat{x},\mathrm{Rx}} \\ s_{\hat{y},\mathrm{Rx}} \end{bmatrix} \approx \begin{bmatrix} s_{\hat{x}} + \rho_{\hat{x}} \cdot s_{\hat{y}} \\ s_{\hat{y}} + \rho_{\hat{y}} \cdot s_{\hat{x}} \end{bmatrix} \tag{20}$$

where for simplicity we have omitted to indicate any short-correlated residual of Φ.

In the formula, $\rho_{\hat{x}}$ and $\rho_{\hat{y}}$ are two complex random processes which may have in general a long-correlated component too, which therefore could be mitigated as well. Similar to the case of NL-PN, the EGN-model correctly estimates the variance of the polarization crosstalk stemming from $\rho_{\hat{x}}$ and $\rho_{\hat{y}}$. However, if such crosstalk is mitigated, then the EGN-model-based estimate of MR may turn out to be pessimistic. As in Sect. IV-A, we are interested in maximizing such discrepancy, i.e., we would like to remove as much polarization crosstalk as possible, to approximately upper bound the error of the EGN-model-based MR estimate in the presence of mitigation. Therefore, we used an idealized mitigator, that we called PolN-Rx, in analogy with the PN-Rx. Similar to the PN-Rx, the idealization consists of assuming full knowledge of the transmitted sequences, $s_{\hat{x}}$ and $s_{\hat{y}}$, for the purpose of estimating $\rho_{\hat{x}}$ and $\rho_{\hat{y}}$. Specifically, we computed:

$$\begin{bmatrix} \tilde{\rho}_{\hat{x}} \\ \tilde{\rho}_{\hat{y}} \end{bmatrix} = \begin{bmatrix} (s_{\hat{x},\mathrm{Rx}} - s_{\hat{x}})/s_{\hat{y}} \\ (s_{\hat{y},\mathrm{Rx}} - s_{\hat{y}})/s_{\hat{x}} \end{bmatrix} \tag{21}$$

The resulting $\tilde{\rho}_{\hat{x}}$ and $\tilde{\rho}_{\hat{y}}$ were filtered through a finite-length integrator, whose integration time was optimized for each simulation, to obtain estimates of the long-correlated components of $\rho_{\hat{x}}$ and $\rho_{\hat{y}}$. We then used such estimates to subtract polarization crosstalk from the signal before final decision and error counting. Note that $\tilde{\rho}_{\hat{x}}$ and $\tilde{\rho}_{\hat{y}}$ contain various disturbances, such as short-correlated NLI, that were omitted above for notational simplicity. Such disturbances should ideally be averaged out by the PolN-Rx.

To show the further gain obtained through the PolN-Rx, when the PN-Rx is also present, we use as model prediction baselines those of Fig. 22, which provide an almost flawless estimate of MR in the presence of the PN-Rx alone. The simulation were then run with the PN-Rx applied first, independently on each polarization, followed by the PolN-Rx. The results are shown in Fig. 23. The mean MR gain between the simulations of Fig. 22, which only have the PN-Rx, to the simulations of Fig. 23, is 2.2% and 3.5%, for the 100 km and 60 km spans landscapes, respectively. Now some gain is obtained also for PM-QPSK, which had gained essentially nothing from the PN-Rx. Overall, however, it appears that polarization crosstalk is a relatively modest effect, at least in the considered system configurations.

In summary, assuming that long-correlated polarization-related non-linear phase-noise has been removed at the CPE stage (the Φ component discussed above), then the mitigation of non-linear polarization *crosstalk* seems to provide only minor MR gains[15]. From a practical end users' viewpoint, it appears that the EGN-model calculated as if the transmitted format was PM-QPSK still provides a rather good MR estimate across the landscape system configurations, even when both the PN-Rx and the PolN-Rx are turned on (Fig. 23).

[15]As a note of caution, this field is currently very active and it may be that more advanced PolN-Rx or even combined PN-PolN-Rx (such as [53]) emerge in the near future, whose effectiveness may be better than that of those used here. So we recommend the readers to monitor the literature for possible developments.

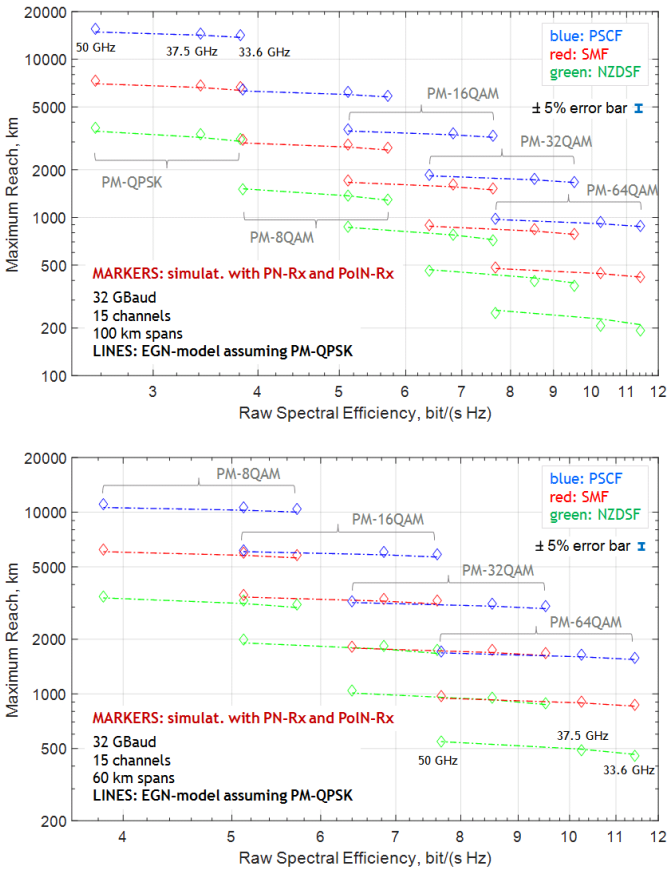

Fig. 23. Dash-dotted lines: prediction of the system maximum reach based on the EGN-model calculated as if PM-QPSK was transmitted in all cases, vs. each system configuration raw spectral efficiency, across the overall test 'landscapes', for span length 100 km (top) and 60 km (bottom). Diamonds: simulation results with both the PN-Rx and the PolN-Rx (i.e., with non-linear phase-noise *and* non-linear polarization crosstalk mitigation) at 33.6, 37.5 and 50 GHz channel spacing.

V. Co-propagating ASE noise and signal depletion

As mentioned earlier, we decided to carry out most of the investigation reported in this paper with ASE noise injected all at the receiver. This was done on purpose, to allow focusing on NLI produced by the signal only. However, in the practical perspective that we declaredly took in this study, the impact on modeling effectiveness of co-propagating ASE noise must be assessed.

Recently, various papers have looked at the modeling implications of co-propagating ASE noise, among which [39] and [27]. Both papers claim that co-propagating ASE starts becoming a factor when the target OSNR at the Rx goes below approximately 9-10 dB. This would make its impact on NLI generation modest for PM-8QAM and perhaps negligible for all higher-order formats. However, PM-QPSK, PS-QPSK (i.e., polarization-switched QPSK), PM-BPSK, as well as other more exotic formats that can operate at lower OSNRs, could actually be substantially impacted.

On the other hand, the industry trend seems to be that lower-OSNR systems than PM-QPSK occupy a very limited niche. This is because, in new plants, PM-QPSK already allows to cover essentially all conceivable planetary distances, even at

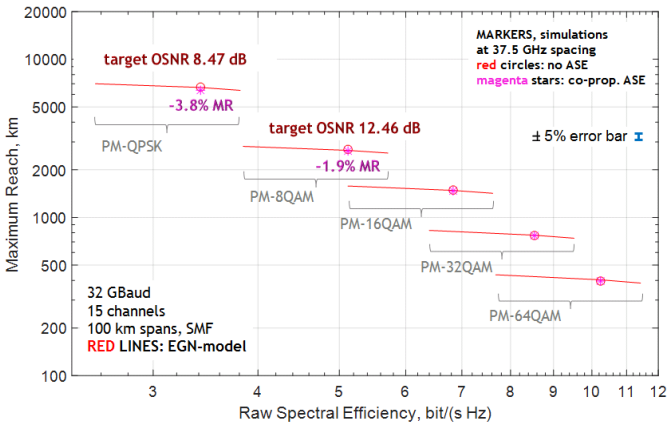

Fig. 24. Red solid lines: prediction of the system maximum reach based on the EGN-model, vs. each system configuration raw spectral efficiency, over SMF with 100 km span length. Red circles: simulation results at 37.5 GHz channel spacing, without co-propagating ASE. Magenta stars: same simulations, *with* co-propagating ASE.

full C or C+L band utilization and quasi-Nyquist spacing. We therefore did not feel it necessary to extend our test landscapes to lower-OSNR systems than PM-QPSK.

In Fig. 24 we show the effect of turning on and off co-propagating ASE, on a subset of the landscape SMF test cases. Clearly, there is no visible impact on PM-64QAM, PM-32QAM or PM-16QAM. Starting with PM-8QAM, some very minor effect is present. With PM-QPSK, the MR decrease nears 4%, at a target OSNR of about 8.5 dB. These data points agree with the results in [39], [27], confirming that above 10 dB of target OSNR the effect can essentially be neglected. Depending on accuracy requirements and target OSNR, it may have to be considered for PM-QPSK, although for many applications this will probably not be necessary. Hence we consider this a relatively minor modeling problem.

In case a correction was absolutely required, a very accurate but complex model, which extends the EGN model to co-propagating ASE, is provided in [27]. Otherwise, [39] proposed an approximate formula (Eq. (7) there), which appears to work well in standard PM-QPSK systems. Despite being simpler, such formula still requires evaluating the EGN-model at each span in the link, which sets its complexity at a very high level. More drastic semi-phenomenological approximations are likely to be possible, which are left for future investigation.

A. Signal depletion

Signal power depletion occurs because NLI is created at the expense of the signal. In fact, if a transparent link is assumed, then whatever optical power is converted to NLI by the Kerr effect, it must come from the signal itself.

The large majority of NLI models is based on perturbation approaches that neglect signal depletion. Both the GN and EGN models neglect it, too. Therefore, when signal depletion is substantial, then a discrepancy may develop between model-based MR predictions and actual system performance.

Similar to what happens with co-propagating ASE, the impact of this phenomenon chiefly depends on the system required target OSNR at the Rx. If the target OSNR is large, then forcedly little NLI can be present at the Rx. This in turn means that signal depletion must be modest. For low target OSNRs, however, signal depletion may be non-negligible.

To get a feeling of what the actual extent of power depletion could be, let us consider a system with a target OSNR of 10 dB. We first remark that *at maximum-reach* the ASE noise power is approximately twice the NLI power (see [40] Sect. 3, or [16] Sect XII-a). Therefore, the signal-to-NLI-noise ratio would be 14.8 dB or, equivalently, NLI would be about 3.4% of the signal power. Assuming a uniform WDM signal, this would result in a signal depletion of approximately the same extent, i.e., 3.4%. At this level, the impact of signal depletion on performance would be marginal. However, upward of this level, it would start having a discernible effect. Therefore, 10 dB target OSNR appears to be a practical threshold for signal depletion needing to be relevant. Note that PM-QPSK routinely operates below 10 dB. Also, powerful FECs or more sensitive formats can actually bring the target OSNR much lower. Therefore, at least for these systems, signal depletion should be accounted for in MR predictions.

Fortunately, there is an easy way to account for signal depletion which, although approximate, appears to work well, at least for uniform WDM signals. It consists of intuitively modifying Eq. (1) as follows:

$$\mathrm{OSNR}_{\mathrm{NL}} = \frac{P_{\mathrm{ch}} - P_{\mathrm{NLI}}}{P_{\mathrm{ASE}} + P_{\mathrm{NLI}}} \tag{22}$$

as proposed for instance in [5] (the factor 'c' there) and recently in [39].

In Fig. 25 we provide some visual appreciation of the difference in MR prediction obtained using either Eq. (1) (solid lines) or Eq. (22) (dashed lines), in the same exact system conditions of Fig. 9 (top). Note that, as already mentioned in footnote 2, we actually used Eq. (22) for all analytical MR predictions calculated in this paper, including Fig. 9, instead of Eq. (1). As pointed out when commenting Fig. 9, the predictions of Eq. (22) very accurately agree with simulations, for all system configurations. Eq. (1) instead overestimates MR. Quantitatively, the difference amounts to about 4.4% overestimation for PM-QPSK, whose target OSNR is 8.5 dB, whereas it is only 1.8% for PM-8QAM whose target OSNR is 12.5 dB. It gets below 1% for PM-16QAM and is negligible for the other formats whose target OSNR is even higher. These results appear to confirm the practical threshold of 10 dB target OSNR, for signal depletion to start impacting MR predictions in a non-negligible way.

In summary, Eq. (22) appears to be a simple and effective correction for signal depletion, at least in the uniform WDM signal configurations tested here. If a very diverse and irregularly spaced WDM comb was used, however, Eq. (22) might lose accuracy. Also, here we tested it down to 8.5 dB OSNR. In [39] some data points are available down to 5 dB, still confirming its effectiveness. If operating at even lower OSNRs, Eq. (22) should be re-tested, to make sure that its validity extends there, too.

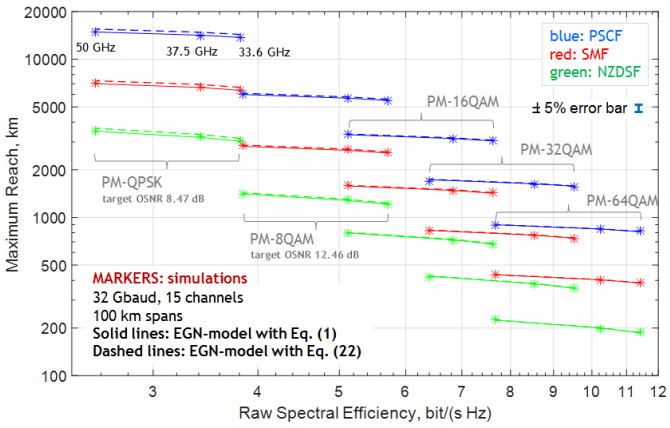

Fig. 25. Lines: prediction of the system maximum reach based on the EGN-model, vs. each system configuration raw spectral efficiency, across the overall test 'landscape', for span length 100 km. *Solid* lines: $\mathrm{OSNR_{NL}}$ computed as in Eq. (1). *Dashed* lines: $\mathrm{OSNR_{NL}}$ computed as in Eq. (22). Star markers: simulation results at 33.6, 37.5 and 50 GHz channel spacing.

VI. NLI MODELING AND DISTRIBUTED AMPLIFICATION

The use of Raman amplification to enhance system performance has been gaining increasingly wider adoption. The currently most popular choice consists of using hybrid Raman/EDFA amplification (HRE). In particular, for various reasons, Raman is mostly used with counter-propagating pumping. Typically, Raman supplies between 40% and 75% of the needed gain. In this section we concentrate first on this more common solution, and then propose a few comments on other distributed-amplification solutions (co-propagating pumping and all-Raman).

HRE is very beneficial as it decreases the equivalent noise figure of the span. Values around 0 dB are possible, for HREs whose EDFA segment has a NF on the order of 4.5 to 5 dB. On the other hand, as the signal power starts to grow back in the last section of the span due to Raman amplification, then some amount of NLI is produced in that section too, which otherwise would contribute no NLI.

Various papers, among which [41], [42], have been published on the topic of finding the best balance of Raman-to-EDFA gain in various system configurations to *maximize performance*, taking into account NLI as well. In this paper, however, we focus instead on *modeling issues*, that is, whether the use of HREs needs special NLI modeling solutions or not.

Fig. 26 shows the normalized power-profile in a span of 100 km of SMF, with total fiber loss 20 dB, with and without Raman amplification, assuming a Raman amplifier gain of 14 dB. Despite the fact that 70% of the span loss is compensated for by the Raman amplifier, the figure strongly suggests that the non-linearity produced at the end of the span may be relatively modest, since NLI depends on signal power cube. Note that there are subtleties, since the strong NLI of the first kilometers of the span then exits the fiber attenuated by almost 6 dB, whereas the weaker NLI of the Raman-amplified last kilometers does not actually undergo any attenuation. At any rate, we tested exactly the configuration of Fig. 26, and the MR results are shown in Fig. 27 for a subset of the landscape

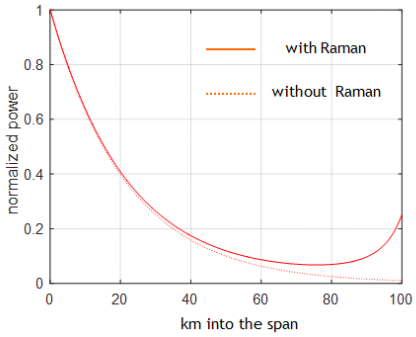

Fig. 26. Normalized signal power-profile in a SMF span of 100 km, with total fiber loss 20 dB, with and without Raman amplification, assuming a Raman amplifier gain of 14 dB.

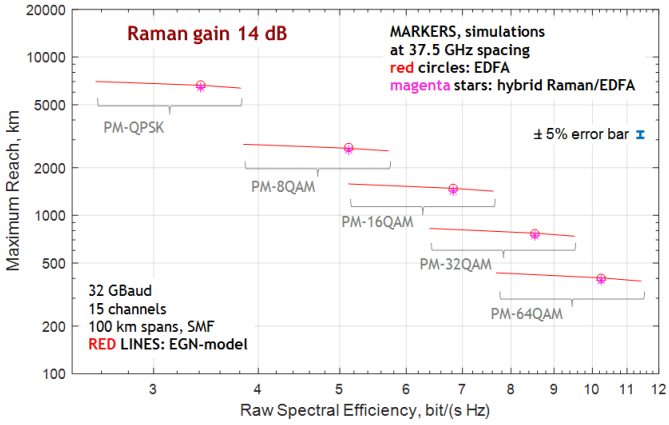

Fig. 27. Red solid lines: prediction of the system maximum reach based on the EGN-model, vs. each system configuration raw spectral efficiency, over SMF with 100 km span length. Red circles: simulation results at 37.5 GHz channel spacing, with 20 dB lumped gain. Magenta stars: same simulations, with with 14 dB Raman gain (counter-propagating pump) and 6 dB lumped gain. The equivalent noise figure (5 dB) was kept the same in the two cases.

systems over SMF.

Since we were specifically interested in gauging the impact of HRE on non-linearity generation, in the simulations we artificially kept the equivalent span NF at the EDFA value (5 dB), both in the case of EDFA-only amplification (red circles) and in the case of HRE (magenta stars). This means that if no extra NLI was produced by the HRE, the same MR would be observed. The clear indication of the figure is that some extra NLI is indeed produced, but the impact is modest, resulting in an average MR decrease of of 3.0%. Notably, all formats appear to be impacted rather uniformly, with minor differences probably attributable to Monte-Carlo uncertainties. Not shown, we plotted a similar graph where the simulations were all run with the PN-Rx turned on. In that case, the average MR loss was less, about 1.5%, which seems to suggest that the excess NLI due to HRE has a larger long-correlated NL-PN content. The fact that distributed-amplification has a greater NL-PN content is in fact in agreement with the results of several papers, among which [24], [33].

In our opinion, these results strongly suggest the MR estimation error incurred by simply neglecting the effect of

HRE is small and acceptable in those system configurations similar to the ones examined here, which appear to be the typically deployed ones. As a practical criterion for neglecting the excess NLI due to HRE, we suggest that the signal must be at least 6 dB lower at the output of a fiber span than at its input or, equivalently, that the Raman section of the HRE leaves at least 6 dB of uncompensated span loss.

However, this criterion is *certainly not met* in the case of *all-Raman* amplified systems, where the power at the output of the fiber span can actually be *greater* than at its input, as some extra gain must be provided to handle the loss of the repeater components (splices, pump couplers, gain-flattening filters, etc.). Assuming lumped amplification in NLI prediction, for an all-Raman system, would lead to substantial error. Similarly, in systems using co-propagating Raman pumping, the power profile is completely different from the usual decreasing exponential. Assuming the latter for the former would, here too, cause substantial NLI prediction errors.

For these scenarios, both the GN-model and the EGN-model provide the mathematical tools to handle the situation. In particular, in both models the power-profile induced by distributed amplification affects only the factor $|\mu|^2$ which, as commented in Sect. II-B, is the non-degenerate-FWM efficiency of the overall link, from input to output. For the special case of backward-pumped Raman amplification, under the assumption of an undepleted pump, an analytical closed-form of $|\mu|^2$ is available ([16], Eq. (10)). Otherwise, $|\mu|^2$ must be found starting from its most general expression, which is reported as Eq. (A8) in Chap. 7 of [2]. Incidentally, the mentioned HRE optimization papers [41], [42] actually resorted to such $|\mu|^2$ expressions accounting for the Raman-gain profile. This of course adds more complexity to the calculations in the GN and especially in the EGN-model. However, at present, to the best of our knowledge, no satisfactory simpler approaches are available.

VII. Other NLI models

As mentioned in Sect. I, many non-linear propagation modeling approaches have been proposed over the years. The most popular models belong to the class of the so-called *regular perturbation (RP) models* [45] and in particular their *first-order* version. Higher-order versions are possible but to the purpose of obtaining system-impact models, first-order versions have typically been used, with few exceptions, such as [43].

Perturbation models based on truncated Volterra Series (VS) have been proposed too, such as [44]. Interestingly, in [45] it was shown that RP models and the VS models are equivalent, so we call them RP-VS models. Other first-order perturbation models, which can be re-conduced or bear substantial similarities to the RP-VS models, were proposed in [46], [47], [48]. As mentioned earlier, the GN end EGN models are first-order RP-VS models, as well. Further perturbation models have also been proposed, such as the logarithmic perturbation (LP) model [49], a combination of the RP and LP model [50], the frequency-resolved LP (FRLP) model [30], [31], the enhanced RP model [12], and still others. We refer the reader to [2] for extended referencing and some broader classification based on the approximations taken.

Many of the above models are similar or nearly equivalent, with some notable exceptions. For instance, LP-models appear to be especially well-suited to study NL-PN. Another example is a *time-domain* RP model derived from [48] and [20], which allows to single-out and assess the amount of long-correlated NL-PN and NL-PolN, according to [51]. In particular, [51] carries out an interesting study of short-haul systems (100-200 km) with very large constellations, employing a combination of a model equivalent to the EGN-model, and the time-domain model mentioned above to correct for possible long-correlated NL-PN and NL-PolN mitigation.

This paper could not possibly test all these different modeling solutions, besides the GN and EGN models. We however advise the reader of the existence of these many other models and it is our auspice that other researcher may carry out selected comparisons of model effectiveness, whose results would certainly benefit the community.

VIII. Comments and conclusion

In this paper we have considered recent advances in the modeling of uncompensated coherent optical systems, focusing on the GN and EGN classes of models. Within these two classes, we have looked at several versions, using different approximations, including semi- or fully-closed-form variants. From our investigation, it is apparent that there is no 'perfect' or 'all-encompassing' solution to NLI modeling in modern uncompensated coherent systems, at least within the considered GN and EGN model classes.

There is however a wide gamut of different answers to specific modeling needs. What is clear is that there are trade-offs, as it could be expected, between accuracy, ease of use and computational complexity. Nonetheless, our results show that several effective solutions are currently available, which represent favorable compromises among the mentioned features.

Which one to pick really depends on the needs of the user. The incoherent GN-model is hard to beat for real-time physical layer awareness and preliminary performance assessments. On the other hand, if very accurate research-oriented investigations need to be carried out, then the full EGN-model, possibly supplemented by other models that allow to precisely assess long-correlated non-linear phase and polarization-noise, such as it was done in [51], must be used.

Several sweet-spot compromises are available in between, whose merits we have tried to highlight. The EGN-model calculated assuming PM-QPSK transmission for all formats, is an effective way of approximately accounting for long-correlated NL-PN mitigation. If computed with the aid of the asymptotic closed-form Eq. (14), it can be a high-accuracy and limited-complexity solution for a wide variety of practical scenarios.

Operation at very low OSNRs, where co-propagating ASE becomes a factor, or with all-Raman amplification, remain tough challenges to date, with modeling solutions only partially satisfactory, due to their complexity.

Research is still ongoing. Judging form the great progress made in just the last few years, it is likely that more effective models will emerge in the near future.

IX. Acknowledgements

The authors would like to thank Gabriella Bosco, Andrea Carena, Vittorio Curri and Fernando Guiomar from Politecnico di Torino, Luca Bertignono and Antonello Nespola from Istituto Superiore Mario Boella, Fabrizio Forghieri, Chris Fludger and Stefano Piciaccia from CISCO Systems, for the fruitful discussions and critical suggestions. The authors would also like to thank Mattia Cantono, Dario Pilori and Marco Bertino from Politecnico di Torino for their invaluable help in setting up the GPU-aided computing resources used for this investigation. Part of the work reported here was previously supported under a sponsored research agreement with CISCO.

Appendix A
List of acronyms

AGN	additive Gaussian noise
AWGN	additive white Gaussian noise
ASE	amplified spontaneous-emission noise
BER	bit error-rate
BP	backward propagation
CD	chromatic dispersion
CPE	carrier-phase estimation
CUT	channel under test
DAC	digital to analog converter
DM	dispersion-managed
DSP	digital signal processing
EDFA	erbium-doped fiber amplifier
EGN-model	enhanced Gaussian-noise model
FEC	forward error-correcting code
FLOP	floating point operation
FWM	four-wave mixing
GN-model	Gaussian-noise model
GNRF	GN-model reference formula
GPU	graphics processing unit
IM/DD	intensity-modulation direct-detection
LOGO	local-optimization, global optimization
ME	Manakov equation
MR	maximum reach
NL	non-linear
NLI	non-linear interference
NL-PN	non-linear phase-noise
NL-PolN	non-linear polarization-noise
NZDSF	non-zero dispersion-shifted fiber
OFDM	orthogonal frequency-division multiplexing
OSNR	optical signal-to-noise ratio
PM	polarization-multiplexed
PMD	polarization-mode dispersion
PSCF	pure-silica-core fiber
PSD	power spectral density
QAM	quadrature amplitude modulation
QPSK	quadrature phase-shift keying
Rx	receiver
SCI	self-channel interference
SE	spectral efficiency
SMF	standard single-mode fiber
SPM	self phase modulation
SRO	symbol-rate optimization
Tx	transmitter
UT	uncompensated transmission, meaning that no optical chromatic dispersion compensation is present in the link
VS	Volterra series
WDM	wavelength-division multiplexing
XPM	cross phase modulation

Appendix B
List of symbols and definitions

- z: the longitudinal spatial coordinate, along the link (km).
- α: fiber *field* loss coefficient (km^{-1}), such that the signal *power* is attenuated as $\exp(-2\alpha z)$.
- β_2: dispersion coefficient in (ps^2·km^{-1})
- γ: no-birefringence fiber Kerr non-linearity coefficient (W^{-1}· km^{-1}). The denomination 'no-birefringence' means that the 8/9 coefficient which dampens the strength of the Kerr non-linearity, stemming from the birefringence-induced polarization wandering along the fiber (see [38]), is not incorporated into γ but rather is included in the coefficients appearing in the $G_{\mathrm{NLI}}(f)$ analytical expressions. Put it differently, in this paper $\gamma = k_0 n_2 / A_{\mathrm{eff}}$, where k_0 is the light wavenumber, n_2 is the non-linear index and A_{eff} is the fiber effective area.
- L_s: span length (km).
- L_{eff}: span effective length (km), defined as $[1 - \exp(-2\alpha L_s)]\,/(2\alpha)$.
- N_s: total number of spans in a link
- Δf: channel spacing, in the case of a uniform WDM signal (THz)
- $G_{\mathrm{WDM}}(f)$: PSD of the overall WDM transmitted signal (W/THz)
- $G_{\mathrm{NLI}}(f)$: PSD of the non-linear interference noise (W/THz)
- P_{ch}: the launch power per channel (W)
- R_s: symbol rate (TBaud)
- *homogeneous link*: a transmission link where all spans are identical (same fiber type, span length and amplification set-up).
- *transparent link*: a transmission link where amplification exactly compensates for fiber loss, span by span.
- *uniform WDM signal*: all channels of the WDM comb have the same symbol rate, the same format, the same spacing and the same launch power.

References

[1] P. Poggiolini, G. Bosco, A. Carena, V. Curri, Y. Jiang, F. Forghieri, 'The GN model of fiber non-linear propagation and its applications,' *J. of Lightw. Technol.*, vol. 32, no. 4, pp. 694-721, Feb. 2014.

[2] P. Poggiolini, Y. Jiang, A. Carena, F. Forghieri, 'Analytical Modeling of the Impact of fiber Non-Linear Propagation on Coherent Systems and Networks,' in *Enabling Technologies for High Spectral-efficiency Coherent Optical Communication Networks*, Xiang Zhou, Chongjin Xie editors, chapter 7, pp. 247-310, ISBN: 978-1-118-71476-8, Wiley, Hoboken (New Jersey), 2016.

[3] A. Splett, C. Kurzke, and K. Petermann, 'Ultimate transmission capacity of amplified optical fiber communication systems taking into account fiber nonlinearities,' *in Proc. ECOC 1993*, vol. 2, pp. 41-44, Montreux (CH), Sept. 1993.

[4] Jau Tang, 'The channel capacity of a multispan DWDM system employing dispersive nonlinear optical fibers and an ideal coherent optical receiver,' *J. Lightwave Technol.*, vol. 20, no. 7, pp. 1095-1101, July 2002.

[5] H. Louchet, A. Hodzic, and Klaus Petermann, 'Analytical model for the performance evaluation of DWDM transmission systems,' *IEEE Phot. Technol. Lett.*, vol. 15, no. 9, pp. 1219-1221, Sept. 2003.

[6] M. Nazarathy, J. Khurgin, R. Weidenfeld, Y. Meiman, Pak Cho, R. Noe, I. Shpantzer, and V. Karagodsky 'Phased-array cancellation of nonlinear FWM in coherent OFDM dispersive multi-span links,' *Optics Express*, vol. 16, pp. 15777-15810, Sept. 2008.

[7] X. Chen and W. Shieh, 'Closed-Form Expressions for Nonlinear Transmission Performance of Densely Spaced Coherent Optical OFDM Systems,' *Optics Express*, vol. 18, pp. 19039-19054, 2010.

[8] P. Poggiolini, A. Carena, V. Curri, G. Bosco, F. Forghieri, 'Analytical Modeling of Non-Linear Propagation in Uncompensated Optical Transmission Links,' *IEEE Photon. Technol. Lett.*, vol. 23, no. 11, pp. 742-744, June 2011.

[9] A. Carena, V. Curri, G. Bosco, P. Poggiolini, F. Forghieri, 'Modeling of the Impact of Non-Linear Propagation Effects in Uncompensated Optical Coherent Transmission Links,' *J. of Lightw. Technol.*, vol. 30, no. 10, pp. 1524-1539, May. 2012.

[10] P. Johannisson and M. Karlsson, 'Perturbation analysis of nonlinear propagation in a strongly dispersive optical communication system,' *J. Lightwave Technol.*, vol. 31, no. 8, pp. 1273-1282, Apr. 15$^{\text{th}}$ 2013.

[11] S. J. Savory, 'Approximations for the nonlinear self-channel interference of channels with rectangular spectra,' *IEEE Phot. Technol. Lett.*, vol. 25, no. 10, pp. 961-964, May 15$^{\text{th}}$ 2013.

[12] P. Serena and A. Bononi, 'An alternative approach to the Gaussian noise model and its system implications,' *J. Lightwave Technol.*, vol. 31, no. 22, pp. 3489-3499, Nov. 15$^{\text{th}}$ 2013.

[13] A. Bononi, O. Beucher, P. Serena 'Single- and cross-channel nonlinear interference in the gaussian noise model with rectangular spectra,' *Optics Express*, vol. 21, no. 26, pp. 32254-32268, Dec. 2013.

[14] P. Johannisson and E. Agrell, 'Modeling of Nonlinear Signal Distortion in Fiber-Optic Networks,' *J. Lightw. Technol.*, vol. 32, no. 23, pp. 45444552, Dec. 2014.

[15] D. Marcuse, C. R. Menyuk, P. K. A. Wai, 'Application of the Manakov-PMD Equation to Studies of Signal Propagation in Optical Fibers with Randomly Varying Birefringence,' *J. Lightwave Technol.*, vol. 15, no. 9, pp. 1735-1746, Sept. 1997.

[16] P. Poggiolini, 'The GN model of non-linear propagation in uncompensated coherent optical systems,' *J. of Lightw. Technol.*, vol. 30, no. 24, pp. 3857-3879, Dec. 2012.

[17] R. Pastorelli, S. Piciaccia, G. Galimberti, E. Self, M. Brunella, G. Calabretta, F. Forghieri, D. Siracusa, A. Zanardi, E. Salvadori, G. Bosco, A. Carena, V. Curri, and P. Poggiolini 'Optical control plane based on an analytical model of non-linear transmission effects in a self-optimized network,' in *Proc. of ECOC 2013*, paper We.3.E.4, London (UK), Sept. 2013.

[18] R. Pastorelli, G. Bosco, A. Nespola, S. Piciaccia, and F. Forghieri, 'Network planning strategies for next-generation flexible optical networks,' in *Proc. OFC 2014*, paper M2B.1, San Francisco (CA), Mar. 2014.

[19] A. Carena, G. Bosco, V. Curri, P. Poggiolini, and F. Forghieri, 'Impact of the transmitted signal initial dispersion transient on the accuracy of the GN-model of non-linear propagation,' in *Proc. of ECOC 2013*, paper Th.1.D.4, London (UK), Sept. 2013.

[20] R. Dar, M. Feder, A. Mecozzi, and M. Shtaif, 'Properties of nonlinear noise in long, dispersion-uncompensated fiber links,' *Optics Express*, vol. 21, no. 22, pp. 25685-25699, Nov. 2013.

[21] A. Carena, G. Bosco, V. Curri, Y. Jiang, P. Poggiolini and F. Forghieri, 'EGN model of non-linear fiber propagation,' *Optics Express*, vol. 22, no. 13, pp. 16335-16362, June 2014. Extended appendices with full formulas derivations can be found in the version available on *www.arXiv.org*

[22] R. Dar, M. Feder, A. Mecozzi, and M. Shtaif, 'Accumulation of nonlinear interference noise in fiber-optic systems,' *Optics Express*, vol. 22, no. 12, pp. 14199-14211, June 2014.

[23] P. Poggiolini, G. Bosco, A. Carena, V. Curri, Y. Jiang, and F. Forghieri, A Simple and Effective Closed-Form GN Model Correction Formula Accounting for Signal non-Gaussian Distribution, *J. of Lightw. Technol.*, vol. 33, no. 2, pp. 459-473, Jan. 2015.

[24] R. Dar, M. Feder, A. Mecozzi, and M. Shtaif 'Inter-Channel Nonlinear Interference Noise in WDM Systems: Modeling and Mitigation,' *J. Lightwave. Technology*, vol. 33, no. 5, pp. 1044-1053, Mar. 2015.

[25] P. Serena, A. Bononi, 'A Time-Domain Extended Gaussian Noise Model,' *J. Lightwave. Technology*, vol. 33, no. 7, pp. 1459-1472, Apr. 2015.

[26] R. Dar, M. Feder, A. Mecozzi, and M. Shtaif 'Pulse collision picture of inter-channel nonlinear interference in fiber-optic communications,' *J. Lightwave. Technology*, vol. 34, no. 2, pp. 593-607, Jan. 2016.

[27] P. Serena, 'Nonlinear SignalNoise Interaction in Optical Links With Nonlinear Equalization,' *J. Lightwave. Technology*, vol. 34, no. 6, pp. 1476-1483, Mar. 2016.

[28] P. Serena and A. Bononi, 'On the accuracy of the Gaussian nonlinear model for dispersion-unmanaged coherent links,' in *Proc. of ECOC 2013*, paper Th.1.D.3, London (UK), Sept. 2013.

[29] P. Poggiolini, A. Nespola, Y. Jiang, G. Bosco, A. Carena, L. Bertignono, S. M. Bilal, S. Abrate, and F. Forghieri, 'Analytical and Experimental Results on System Maximum Reach Increase Through Symbol Rate Optimization,' *J. of Lightw. Technol.*, vol. 34, no. 8, pp. 1872-1885, Apr. 2016.

[30] M. Secondini, E. Forestieri, 'Analytical Fiber-Optic Channel Model in the Presence of Cross-Phase Modulation', *IEEE Phot. Technol. Lett.*, vol. 24, pp. 2016-2019, Nov. 2012.

[31] M. Secondini, E. Forestieri, G. Prati, 'Achievable information rate in nonlinear WDM fiber-optic systems with arbitrary modulation formats and dispersion maps,' *J. Lightwave Technol.*, 31, 38393852 (2013).

[32] Y. Jiang, A. Carena, P. Poggiolini, and F. Forghieri, 'On the impact of non-linear phase-noise on the assessment of long-haul uncompensated coherent systems performance,' in *Proc. of ECOC 2014*, Cannes (FR), Sept. 2014.

[33] M. Secondini, E. Forestieri, 'On XPM Mitigation in WDM Fiber-Optic Systems', PTL, vol. 26, pp. 2252- 2255, Nov. 2014.

[34] T. Fehenberger, N. Hanik, T. A. Eriksson, P. Johannisson, M. Karlsson, 'On the Impact of Carrier Phase Estimation on Phase Correlations in Coherent Fiber Transmission,' 2015 Tyrrhenian International Workshop on Digital Communications (TIWDC), available on IEEE Xplore.

[35] Carsten Schmidt-Langhorst, Robert Elschner, Felix Frey, Robert Emmerich, Colja Schubert, 'Experimental Analysis of Nonlinear Interference Noise in Heterogeneous Flex-Grid WDM Transmission,' in *Proc. of ECOC 2015*, paper Tu.1.4.3, Sept. 2015.

[36] T. Fehenberger, M. P. Yankov, L. Barletta, and N. Hanik, 'Compensation of XPM interference by blind tracking of the nonlinear phase in WDM systems with QAM input,' in *Proc. of ECOC 2015*, paper Th.1.D.4, Valencia (ES), Sept. 2015.

[37] A. Nespola, L. Bertignono, G. Bosco, A. Carena, P. Poggiolini, F. Forghieri 'Independence of the Impact of Inter-Channel Non-Linear Effects on Modulation Format and System Implications,' in *Proc. of ECOC 2016*, Dusseldorf (DE), Sept. 2016.

[38] D. Wang, C. R. Menyuk, 'Polarization Evolution Due to the Kerr Nonlinearity and Chromatic Dispersion', *J. of Lightw. Technol.*, vol. 17, no. 12 , pp. 2520-2529, Dec. 1999.

[39] P. Poggiolini, A. Carena, Y. Jiang, G. Bosco, V. Curri, and F. Forghieri, Impact of low-OSNR operation on the performance of advanced coherent optical transmission systems, in *Proc. of ECOC 2014*, paper Mo.4.3.2, Cannes (FR), Sept. 2014. Available with corrections at www.arXiv.org, paper arXiv:1407.2223.

[40] E. Grellier, A. Bononi, 'Quality parameter for coherent transmissions with Gaussian-distributed nonlinear noise,' *Optics Express*, vol. 19, no. 13, pp. 12781-12788, June 2011.

[41] V. Curri, A. Carena, P. Poggiolini, G. Bosco, F. Forghieri, 'Extension and validation of the GN model for non-linear interference to uncompensated links using Raman amplification,' *Optics Express*, vol. 21., no. 3, pp. 3308-3317, Feb. 2013.

[42] V. Curri, A. Carena, 'Merit of Raman pumping in uniform and uncompensated links supporting NyWDM', *J. Lightwave Technol.*, vol. 34, no. 2, pp. 554-565, Jan. 2016.

[43] S. Kumar and D. Yang, Second-order theory for self-phase modulation and cross-phase modulation in optical fibers, *J. Lightwave Technol.*, vol. 23, no. 6, pp. 2073-2080, June 2005.

[44] K.V. Peddanarappagari and M. Brandt-Pearce Volterra series transfer function of single-mode fibers, *J. of Lightwave. Technol.*, vol. 15, no. 12, pp. 2232-2241, Dec. 1997.

[45] A. Vannucci, P. Serena, and A. Bononi, The RP method: a new tool for the iterative solution of the nonlinear Schrodinger equation, *J. Lightwave Technol.*, vol. 20, no. 7, pp. 1102-1112, July 2002.

[46] A. Mecozzi, C. Balslev Clausen, and M. Shtaif, Analysis of intrachannel nonlinear effects in highly dispersed optical pulse transmission, *Photon. Technol. Lett.*, vol. 12, no. 4, pp. 392-394, Apr. 2000.

[47] E. E. Narimanov and P. P. Mitra, The channel capacity of a fiber optics communication system: perturbation theory, *J. Lightwave Technol.*, vol. 20, no. 3, pp. 530-537, Mar. 2002.
[48] A. Mecozzi, R.-J. Essiambre, 'Nonlinear Shannon limit in pseudolinear coherent systems,' *J. Light. Tech.*, vol. 30, no. 12, pp. 20112024, June 2012.
[49] E. Forestieri and M. Secondini, Solving the non-linear Schroedinger equation, in *Optical Communication Theory and Techniques*, Boston: Springer, 2005, pp. 3-11.
[50] M. Secondini, E. Forestieri, and C. R. Menyuk, A combined regular-logarithmic perturbation method for signal-noise interaction in amplified optical systems, *J. Lightwave Technol.*, vol. 27, no. 16, pp. 3358-3369, Aug. 2009.
[51] R. Dar, P. Winzer 'On the Limits of Digital Back-Propagation in Fully Loaded WDM Systems,' *Photon. Technol. Lett.*, vol. 12, no. 4, pp. 392-394, Apr. 2000.
[52] Chongjin Xie, 'Local Oscillator Phase Noise Induced Penalties in Optical Coherent Detection Systems Using Electronic Chromatic Dispersion Compensation,' in *Proc. of OFC 2009*, paper OMT4, San Diego (CA), Mar. 2009.
[53] C. B. Czegledi, E. Agrell, M. Karlsson, P. Johannisson, 'Modulation Format Independent Joint Polarization and Phase Tracking for Coherent Receivers,' *J. Lightw. Technol.*, vol. 34, no. 14, pp. 3354 -3364, July 2016.